Tubular hydrogel pumps through a responsive LENS

Joseph J. Webber† and Thomas D. Montenegro-Johnson

Mathematics Institute, University of Warwick, Coventry CV4 7AL, UK

(Received xx; revised xx; accepted xx)

Thermo-responsive hydrogels are smart materials that can rapidly switch between hydrophilic (swollen) and hydrophobic (shrunken) states when heated past a threshold temperature. This switch results in order-of-magnitude changes in gel volume, allowing for the construction of microfluidic devices or smart actuators. However, modelling thermo-responsive hydrogels is difficult, and typically involves fitting a large number of material parameters to tune the model to experimental data. In this paper, we extend the intuitive and inherently macroscopic linear-elastic-nonlinear-swelling (LENS) model of Webber & Worster (*J. Fluid Mech*, vol. 96, 2023, A37) to incorporate thermo-responsivity. We show how temperature affects the osmotic pressure of a gel and therefore modifies the equilibrium polymer fraction. Using this model, we then consider hollow tubes of thermo-responsive hydrogel immersed in water, which deswell when heated, pumping fluid as the tube collapses. Such tubes may be able to act as effective "on-board" displacement pumps on smart microfluidic devices, removing the need for bulky pressure-driven syringe pumps. We finally show how the response times and flow characteristics in the tubes may be easily modified by varying the geometry or material properties of the hydrogel, allowing for faster response times in larger-scale devices and unlocking new possibilities for dynamic shape change.

Key words: Authors should not enter keywords on the manuscript, as these must be chosen by the author during the online submission process and will then be added during the typesetting process (see Keyword PDF for the full list). Other classifications will be added at the same time.

1. Introduction

Hydrogels are soft porous materials comprising a cross-linked, hydrophilic, polymer structure surrounded by adsorbed water molecules that are free to move through the porous scaffold (Doi 2009; Bertrand *et al.* 2016; Webber & Worster 2023). Though simple in structure, their elastic and soft nature, coupled with the ability to change volume to an extreme degree by swelling or drying, affords them a number of uses in engineering, medical sciences and agriculture (Zohuriaan-Mehr *et al.* 2010; Guilherme *et al.* 2015). In addition to these applications of 'passive' hydrogels, all based on the composition or large-swelling behaviour

† Email address for correspondence: joe.webber@warwick.ac.uk

of such materials, so-called responsive hydrogels have also been developed, where the affinity of the polymer scaffold for water changes as a result of external stimuli such as heat, light or chemical concentration (Neumann *et al.* 2023).

In recent years, interest in 'smart' materials with controllable shape changing behaviour has increased, with implementations in soft robotics (Lee *et al.* 2020), microfluidics (Dong & Jiang 2007), and in models of biological processes (Vernerey & Shen 2017). Though responsive gels can react to stimuli of various forms, the most ubiquitous are thermo-responsive gels, where the affinity of the polymer chains for water drops rapidly at a critical temperature T_C. Above this lower critical solution temperature (LCST), hydrogen bonds holding the water molecules in place around the polymer chains break, and release of water molecules is entropically favoured. There exist a number of polymers which can form such responsive gels, but since the critical deswelling temperature of poly(*N*-isopropylacrylamide) (PNIPAM) can be tuned to be close to room temperature, this is a common material choice for applications involving responsive gels (Butler & Montenegro-Johnson 2022). The effect of deswelling is significant, with many such gels exhibiting an order-of-magnitude volume change at T_C, opening up the possibility of a number of macroscopic use cases for responsive gels (Voudouris *et al.* 2013).

In order to model the response of gels to changes in temperature, many authors seek the dependence of the Helmholtz free energy on the ambient temperature. This is encoded by the Flory χ parameter, representing the attraction between water molecules and polymer chains. This parameter typically decreases with increasing temperature (Cai & Suo 2011), but its value is usually deduced from fitting (Afroze *et al.* 2000). Accurately determining the χ parameter is a long-standing problem in polymer physics, with experimental approaches often difficult, owing to the number of different physical processes underpinning solvent–polymer and polymer–polymer interactions, with some more recent work using machine learning approaches (Nistane *et al.* 2022) to seek patterns in the variation of χ with polymer structure. It is, nonetheless, an important pursuit, since small changes in χ can lead to large differences in the physics of hydrogels.

Given an expression for the Helmholtz free energy, it can then be minimised with respect to deformation to allow the equilibrium swelling state at a fixed temperature to be determined. However, describing the transient evolution of the state of the hydrogel as the temperature is varied is significantly more difficult, and requires the separate consideration of chemical potentials, polymer network elasticity and induced interstitial flows through the gel. In traditional large-strain poroelastic modelling Bertrand *et al.* (2016), the principal stresses (in the directions of the principal stretches) are deduced from the energy, and these are then balanced with gradients in chemical potential to describe the poroelastic flow, and thus the evolution of the gel, in time. The potential for such a formulation to admit analytical solutions is limited.

While effective, these models rely on a characterisation of the material in terms of a large number of microscopic parameters, are computationally expensive, and result in a series of coupled partial differential equations for porosity, chemical potential and stresses, which potentially masks some of the key macro-scale physics driving the responsive dynamics. For these reasons, we seek a model based only on macroscopically-measurable material properties to give faster predictions to describe the transient swelling-deswelling states in response to temperature changes. Since many of the applications of these responsive gels are to systems such as small microfluidic devices (Harmon *et al.* 2003) or robotic actuators (Lee *et al.* 2020), being able to predict behaviour accurately with few parameters and with the existence of analytical solutions is of great importance.

It is possible to model the behaviour of deformable soft porous media using the theory of linear poroelasticity, characterising the gel by its elastic moduli and describing the flow

through the scaffold using Darcy's law (Doi 2009). These models are analytically-tractable and macroscopic in nature. However, they cannot cope with nonlinearities that arise from large swelling strains, and are therefore unsuitable for modelling super-absorbent gels, where the volumetric changes involved in swelling and drying may be of the order of 10 to 100 times (Bertrand *et al.* 2016).

Swelling and drying involve isotropic deformation of the polymer scaffold, however, and it is reasonable to assume that, at any swelling state, the hydrogel material acts as a linear-elastic bulk solid. In Webber & Worster (2023) and Webber *et al.* (2023), a model is introduced that allows for nonlinearities in the isotropic strain but linearises around small deviatoric strains, allowing for us to reduce the gel dynamics to a nonlinear advection-diffusion equation for the local polymer (volume) fraction ϕ. The model characterises any gel in terms of three material parameters, all of which depend on polymer fraction: a shear modulus $\mu_s(\phi)$ characterising resistance to shear deformation; a permeability $k(\phi)$ describing the viscous resistance to flow through the scaffold; and an osmotic modulus $\Pi(\phi)$ encoding the affinity between water and polymer molecules. In this paper, we incorporate thermo-responsive effects in the above linear-elastic-nonlinear-swelling model by assuming that the osmotic pressure (and potentially other material parameters) can depend also on temperature. This dependency leads to different swelling behaviour as the temperature is varied, and different equilibrium states either side of the LCST.

We begin with the Helmholtz free energy derived from Flory-Huggins theory and neo-Hookean elasticity of polymer chains, commonly used in models for active gel behaviour. This approach is used widely in the thermo-responsive gels literature, and has been seen to provide an accurate description of the swelling and deswelling processes (Cai & Suo 2011; Butler & Montenegro-Johnson 2022). From this starting position, in section 2 we derive a stress tensor and identify the osmotic modulus and shear modulus, for temperature T, polymer fraction ϕ, and combinations of the parameters commonly used in nonlinear models. Using literature values for these parameters, our reduced model is able to reproduce key results and observations from the fully nonlinear models.

The utility of such a tractable model is found in its ability to apply to a number of more complicated physical settings and provide good qualitative and quantitative predictions of the key physics at play. Such examples are seen in soft robotic and microfluidic devices where the geometry changes in response to an external stimulus, or where changes in geometry pump solvent fluid from one place to another. Hydrogels have long been proposed as ideal materials to achieve this in microfluidic devices, either through functioning as valves (Dong & Jiang 2007), as passive pumps (drawing in water through their swelling behaviour) (Seo *et al.* 2019), or indeed as displacement pumps (Richter *et al.* 2009). It is this latter behaviour that we model here, considering the contraction of a hollow tube formed of thermo-responsive hydrogel when a heat pulse is applied, and using the thermo-responsive linear-elastic-nonlinear-swelling model derived in section 2 to deduce both the shrunken geometry and the transition from swollen to shrunken states by the flow of water through the hydrogel walls and the hollow lumen of the 'pipe'.

Notably, the presence of a fluid-filled pore in the centre of a tube allows for much faster responses to changes in temperature than in a pure gel, since the flow that results from deswelling is not restricted by viscous resistance through the pore matrix. Our model gives expressions for the pumping rate and characteristics of the induced peristaltic fluid flow in response to propagating heat pulses.

In addition to applications driving fluid flow in microfluidic devices, a number of existing applications depend on the ability to tune response times to external stimuli (Maslen *et al.* 2023). In such constructions, anisotropic shape changes result from isotropic deswelling that occurs at different rates - so-called "dynamic anisotropy" - in response to a heat pulse.

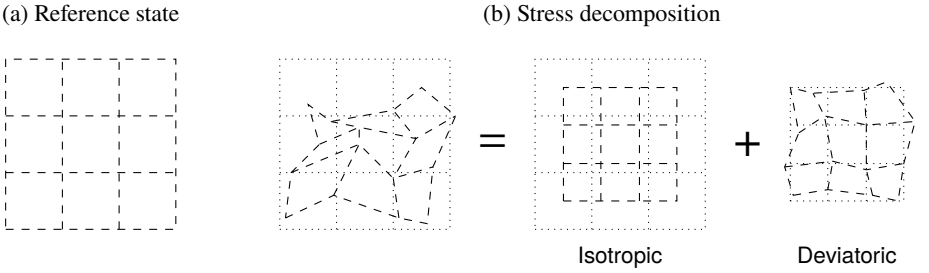

Figure 1: On the left, the reference state where $\phi \equiv \phi_0$ and the cross-linked polymers are in thermodynamic equilibrium with the surroundings. On the right, a schematic decomposition of any deformation (dashed lines) from this reference state (dotted lines) into an isotropic part due to drying (in this case) and a small deviatoric part.

This behaviour is key to unlocking non-reciprocal shrinking-swelling dynamics, critical for achieving work in the inertialess fluid regime. The existence of a simplified, analytic, understanding of thermo-responsive gels allows us to tune the thickness of the pipe walls to give a desirable response time, allowing for the construction of responsive hydrogel devices with controllable response rates to external stimuli, irrespective of the intrinsic material response rate.

2. Thermo-responsive linear-elastic-nonlinear-swelling model

The linear-elastic-nonlinear-swelling (henceforth LENS) model introduced in Webber & Worster (2023) and Webber *et al.* (2023) is a poromechanical continuum model for the behaviour of large-swelling gels. The model is derived based upon the assumption that isotropic strains, corresponding to the swelling and drying of a gel, may be large, but deviatoric strains must be small. Figure 1 shows how a general deformation from a reference state can be decomposed into these two parts, and illustrates how we can view isotropic shrinkage or growth as drying or swelling, respectively. In other words, at any given degree of swelling, a hydrogel is modelled as a linear-elastic material with 'macroscopic' parameters, dependent on its degree of swelling. These parameters characterise both the elastic response and the flow of interstitial water. In general, we expect drier gels (with a higher local polymer fraction) to be stiffer and less permeable.

In the LENS model, the degree of swelling is quantified by the local polymer (volume) fraction ϕ, and all deformation is measured relative to a uniformly-swollen reference state where $\phi \equiv \phi_0$, the free-swelling equilibrium (figure 1a). If gel elements in the reference state are labelled by the Lagrangian coordinates $\boldsymbol{X}$, any deformation of the gel can be described by a mapping to Eulerian coordinates $\boldsymbol{x}$. The deformation gradient tensor $\boldsymbol{F}$ is defined as the backwards derivative of the Eulerian coordinates relative to the Lagrangian ones (Reddy 2013), and has components

$$\mathsf{F}_{ij} = \frac{\partial x_i}{\partial X_j}, \tag{2.1}$$

with the volumetric change of a deformation being given by $J = \det \boldsymbol{F}$. Volume can only change via movement of water into or out of the polymer scaffold, since both phases are considered to be separately incompressible, and therefore $J = (\phi/\phi_0)^{-1}$. The governing assumption of the LENS model is that the deformation described by $\boldsymbol{F}$ is, at leading order,

isotropic and swelling-driven, so that

$$\boldsymbol{F} = \left(\frac{\phi}{\phi_0}\right)^{-1/3} \boldsymbol{I} + \boldsymbol{f}, \tag{2.2}$$

with all components f_{ij} small. Measuring displacements $\boldsymbol{\xi} = \boldsymbol{x} - \boldsymbol{X}$ relative to the equilibrium, a Cauchy strain tensor $\boldsymbol{e}$ can be defined with

$$\boldsymbol{e} = \frac{1}{2}\left[\boldsymbol{\nabla}\boldsymbol{\xi} + (\boldsymbol{\nabla}\boldsymbol{\xi})^{\mathrm{T}}\right] = \boldsymbol{I} - \frac{1}{2}\left(\boldsymbol{F} + \boldsymbol{F}^{\mathrm{T}}\right)^{-1} = \left[1 - \left(\frac{\phi}{\phi_0}\right)^{1/3}\right]\boldsymbol{I} + \epsilon, \tag{2.3}$$

using the Taylor series expansion for the inverse of a nearly-diagonal matrix (Petersen & Pedersen 2012), where

$$\epsilon = \frac{1}{2}\left(\frac{\phi}{\phi_0}\right)^{2/3}\left(\boldsymbol{f} + \boldsymbol{f}^{\mathrm{T}}\right) + O(\boldsymbol{f}^2) \tag{2.4}$$

is the (small) deviatoric strain. The isotropic strain can be seen to be related solely to changes in polymer fraction, via the volumetric expansion factor J (Webber & Worster 2023). Central to LENS modelling is the constitutive relation for the Cauchy stress tensor

$$\sigma = -\left[p + \Pi(\phi)\right]\boldsymbol{I} + 2\mu_s(\phi)\epsilon, \tag{2.5}$$

relating deformation of the hydrogel to stresses. Here, there is a deviatoric 'shear stress' term arising from deviatoric strain and governed by the shear modulus $\mu_s(\phi)$ and a term dependent on the bulk pressure $P = p + \Pi(\phi)$.

The bulk pressure P is split into a contribution from the pervadic pressure p (Peppin *et al.* 2005) and the generalised osmotic pressure $\Pi(\phi)$. The pervadic pressure is akin to the chemical potential in other models (Bertrand *et al.* 2016; Butler & Montenegro-Johnson 2022), and defined to be the pressure of the fluid component as would be measured behind a partially-permeable membrane that only allows fluid to pass. It is gradients in p that drive flow through the interstices of the gel matrix, via Darcy's law

$$\boldsymbol{u} = -\frac{k(\phi)}{\mu_l}\boldsymbol{\nabla} p, \tag{2.6}$$

where $k(\phi)$ is the permeability (which we expect to decrease with increasing polymer fraction) and μ_l is the fluid viscosity. Meanwhile, the generalised osmotic pressure (henceforth simply the osmotic pressure) $\Pi(\phi)$ is given by $\Pi = P - p$ and has contributions both from mixing of the polymer and water phases and isotropic elasticity of the scaffold, representing the affinity of the gel for water.

Coupled with conservation equations for water and polymer, interstitial flows lead to swelling and drying, processes which can be described by the advection-diffusion equation

$$\frac{\partial \phi}{\partial t} + \boldsymbol{q}\cdot\boldsymbol{\nabla}\phi = \boldsymbol{\nabla}\cdot\left[D(\phi)\boldsymbol{\nabla}\phi\right] \quad \text{with} \quad D(\phi) = \frac{k(\phi)}{\mu_l}\left[\phi\frac{\partial \Pi}{\partial \phi} + \frac{4\mu_s(\phi)}{3}\left(\frac{\phi}{\phi_0}\right)^{1/3}\right], \tag{2.7}$$

where $\boldsymbol{q}$ is a phase-averaged flux vector equal to the sum of polymer velocity (the rate of deformation of the scaffold) and interstitial fluid flux. In Webber & Worster (2023) it is further shown that whenever the assumptions of small deviatoric strain are made, all behaviour can be described in terms of $\boldsymbol{\xi}$ and ϕ through

$$\boldsymbol{u} = \frac{D(\phi)}{\phi}\boldsymbol{\nabla}\phi, \quad \boldsymbol{\nabla}\cdot\boldsymbol{q} = 0 \quad \text{and} \quad \boldsymbol{q} = \frac{D(\phi)}{\phi}\boldsymbol{\nabla}\phi + \left(\frac{\phi}{\phi_0}\right)^{-1/3}\frac{\partial \boldsymbol{\xi}}{\partial t}. \tag{2.8}$$

Therefore, the response of any gel can be characterised by three material parameters: an osmotic pressure $\Pi(\phi)$, a shear modulus $\mu_s(\phi)$ and a permeability $k(\phi)$, all of which influence the polymer diffusivity $D(\phi)$ of equation (2.7). A key foundation of the LENS approach is that these three parameters are macroscopically-measurable and there is no discussion of the microscopic processes – such as the electrostatic attraction between water and polymer molecules or the entropic contributions from mixing – that govern these observable properties. However, given a model for the microscopic-scale interactions, the material properties can be determined. For example, the model of Cai & Suo (2012) is used to derive expressions for $\Pi(\phi)$ and $\mu_s(\phi)$ in the limit of small deviatoric strains in an appendix of Webber & Worster (2023), allowing us to then use the LENS formalism for gel dynamics, based on the physics captured by this particular expression for the Helmholtz free energy.

In the present study, we will assume that $k(\phi) = k$, a constant, for simplicity, even though we expect permeability to decrease as polymer fraction increases. This approach is taken by other authors, including Butler & Montenegro-Johnson (2022), who note that incorporating a ϕ-dependent permeability leads to few qualitative differences from cases where it does not vary as the gel swells or dries. We instead seek the dependence of the remaining two material parameters on the ambient temperature, explaining the qualitative changes to hydrogel behaviour as the critical temperature threshold for deswelling, $T = T_C$, is crossed.

2.1. *Thermodynamic models for thermo-responsive hydrogels*

In order to describe responsive hydrogels in the context of our LENS model, a reference state that is independent of temperature must be introduced. In the present study, we consider a reference temperature T_0 (well below the LCST threshold T_C for deswelling), and define the reference state as the uniformly swollen state attained by an unconstrained gel left to swell in an excess of water at $T = T_0$, where $\phi \equiv \phi_{00}$.

As the temperature changes, the equilibrium polymer fraction $\phi_0(T)$ will also change, with ϕ_0 being greater above the critical temperature T_C, and lower below; in other words, the gel swells to a greater degree at lower temperatures. We write the reference equilibrium polymer fraction as $\phi_0(T_0) = \phi_{00}$. The equilibrium value is reached in the absence of any stresses in the gel, and so the osmotic pressure $\Pi(\phi_0) = 0$ at any temperature.

In Butler & Montenegro-Johnson (2022), the standard energy density function for a thermo-responsive hydrogel (Cai & Suo 2011) is used, following Flory-Huggins mixture theory and a neo-Hookean elastic model for the polymer chains,

$$\mathcal{W} = \frac{k_B T}{2\Omega_p}\left[\mathrm{tr}\left(\boldsymbol{F_d}\boldsymbol{F_d}^T\right) - 3 + 2\log\phi\right] + \frac{k_B T}{\Omega_f}\left[\frac{1-\phi}{\phi}\log(1-\phi) + \chi(\phi, T)(1-\phi)\right], \quad (2.9)$$

where $\boldsymbol{F_d}$ is the deformation gradient tensor measured relative to a fully-dry polymer, the same as the $\boldsymbol{F}$ defined above if ϕ_0 were equal to unity. We can rewrite $\boldsymbol{F_d}$ in terms of $\boldsymbol{F}$, the deformation gradient measured relative to a state where $\phi \equiv \phi_{00}$, since the transition between the two states can be described by an isotropic scaling transformation,

$$\boldsymbol{F_d} = \left(\phi_{00}^{-1/3}\boldsymbol{I}\right)\boldsymbol{F} = \phi_{00}^{-1/3}\boldsymbol{F} \quad \text{so} \quad \mathrm{tr}\left(\boldsymbol{F_d}\boldsymbol{F_d}^T\right) = \phi_{00}^{-2/3}\mathsf{F}_{ab}\mathsf{F}_{ab}, \quad (2.10)$$

using Einstein summation convention. Following the approach of Cai & Suo (2012), the Terzaghi effective stress tensor $\sigma^{(e)}$ (i.e. $\sigma + p\boldsymbol{I}$) has components given by

$$\sigma^{(e)}_{ij} = \phi\frac{\partial\mathcal{W}}{\partial\mathsf{F}_{ik}}\mathsf{F}_{jk}, \quad (2.11)$$

again using summation convention. This derivation is usually based on the assumption of a

spatially-uniform and constant temperature field, though appendix A justifies its use for the cases we are considering here. Since $\det \boldsymbol{F} = \phi_{00}/\phi$, the expression for the derivative of a determinant with respect to a matrix (Petersen & Pedersen 2012) implies that

$$\frac{\partial \phi}{\partial \mathsf{F}_{ik}} = -\phi \mathsf{F}^{-1}_{ki}. \tag{2.12}$$

Hence,

$$\frac{\partial \mathcal{W}}{\partial \mathsf{F}_{ik}} = \frac{k_B T}{\Omega_f}\left\{\frac{1}{\Omega\phi_{00}^{2/3}}\mathsf{F}_{ik} + \left[\frac{\log(1-\phi)}{\phi} + 1 + \phi\chi(\phi, T) - \phi(1-\phi)\frac{\partial \chi}{\partial \phi} - \frac{1}{\Omega}\right]\mathsf{F}^{-1}_{ki}\right\} \text{ and}$$

$$\sigma^{(e)}_{ij} = \frac{k_B T}{\Omega_f}\left\{\left[\log(1-\phi) + \phi + \phi^2\chi - \phi^2(1-\phi)\frac{\partial \chi}{\partial \phi} - \frac{\phi}{\Omega}\right]\delta_{ij} + \frac{\phi}{\Omega\phi_{00}^{2/3}}\mathsf{F}_{ik}\mathsf{F}_{jk}\right\}, \tag{2.13}$$

where $\Omega = \Omega_p/\Omega_f$ represents the volume of polymer molecules relative to solvent molecules. Using the expansion of equation (2.2) and the deviatoric strain expression (2.4),

$$\mathsf{F}_{ik}\mathsf{F}_{jk} = \left(\frac{\phi}{\phi_{00}}\right)^{-2/3}\delta_{ij} + \frac{2\phi_{00}}{\phi}\epsilon_{ij}, \tag{2.14}$$

and so the two temperature-dependent material parameters are

$$\Pi(\phi) = \frac{k_B T}{\Omega_f}\left[\Omega^{-1}\left(\phi - \phi^{1/3}\right) - \phi - \log(1-\phi) - \phi^2\chi + \phi^2(1-\phi)\frac{\partial \chi}{\partial \phi}\right] \quad \text{and} \tag{2.15a}$$

$$\mu_s(\phi) = \frac{k_B T \phi_{00}^{1/3}}{\Omega_p}. \tag{2.15b}$$

Notice that the shear modulus is independent of polymer fraction, and increases with temperature and chain length (longer polymer chains have a larger Ω_p). The temperature-dependence of the osmotic pressure is more complicated, with contributions from the $k_B T$ prefactor, χ, and $\partial\chi/\partial\phi$.

2.2. *Equilibrium polymer fraction*

As discussed above, the equilibrium polymer fraction $\phi_0(T)$ is found by setting the osmotic pressure (2.15*a*) to zero. In the present study, we follow Butler & Montenegro-Johnson (2022) in specifying an interaction parameter that depends linearly on both ϕ and T,

$$\chi(\phi, T) = A_0 + B_0 T + (A_1 + B_1 T)\phi, \tag{2.16}$$

where the four parameters can be fitted to existing models in the literature. Here, we consider two example models – the first is based on Afroze *et al.* (2000) (ANB), and the second is based on Hirotsu *et al.* (1987) and henceforth referred to as HHT. The fitting parameters, as found in Butler & Montenegro-Johnson (2022), are summarised in table 1.

To find the equilibrium polymer fraction, we consider the expression

$$\Omega^{-1}\left(\phi_0 - \phi_0^{1/3}\right) - \phi_0 - \log(1-\phi_0) - \phi_0^2\left[A_0 + B_0 T + (2\phi_0 - 1)(A_1 + B_1 T)\right] = 0, \tag{2.17}$$

for the two choices of parameters, and figure 2 shows the variation of ϕ_0 with temperature in both the ANB and HHT parameter sets. In the case of the parameters of Afroze *et al.* (2000), it is especially apparent that there are two critical temperatures. As the temperature is lowered from around 310 K, and the equilibrium polymer fraction ϕ_0 decreases (swelling), there is a rapid increase in swelling at $T_C^{\uparrow} \approx 304.5\,\mathrm{K}$, the swelling critical temperature.

Model	A_0	A_1	B_0	B_1	Ω
ANB (Afroze *et al.* 2000)	−12.947	17.92	$0.04496\,\mathrm{K}^{-1}$	$-0.0569\,\mathrm{K}^{-1}$	100
HHT (Hirotsu *et al.* 1987)	−62.22	−58.28	$0.20470\,\mathrm{K}^{-1}$	$0.19044\,\mathrm{K}^{-1}$	720

Table 1: Fitted parameter values for the two thermo-responsive hydrogels considered in Butler & Montenegro-Johnson (2022), based on two pre-existing models from the literature.

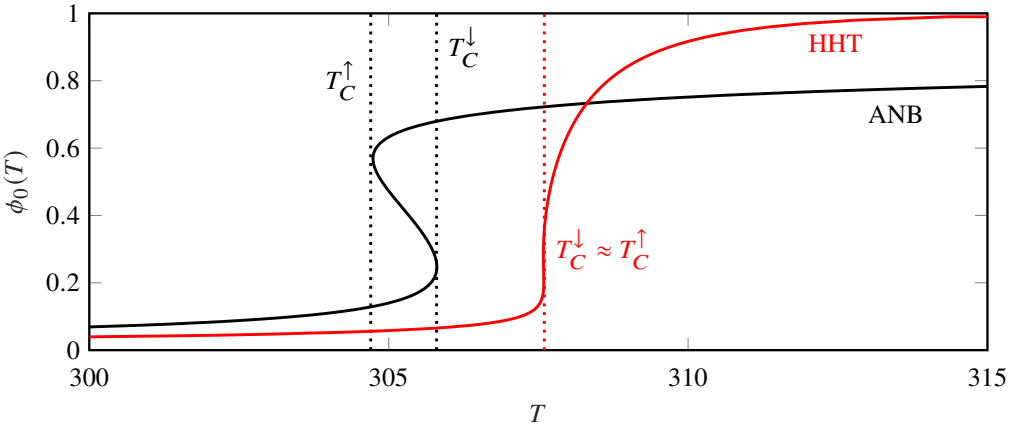

Figure 2: Plots of the equilibrium polymer fraction, determined by $\Pi(\phi_0) = 0$ in equation (2.17). Two choices of parameter values are plotted; those determined by Afroze *et al.* (2000) (ANB) and Hirotsu *et al.* (1987) (HHT), showing the volume phase transition temperatures for swelling ($T_C^{\uparrow}$) and shrinking ($T_C^{\downarrow}$), respectively.

As the temperature is increased from around 300 K, however, there is a different critical temperature, $T_C^{\downarrow} \approx 306\,\mathrm{K}$ at which there is rapid drying. This hysteresis is in fact exhibited in the case of both sets of parameters, where there are multiple solutions in a narrow band of temperatures around the critical volume phase transition temperature T_C, an effect which we ignore in the present study, modelling the equilibrium polymer fraction as single-valued at any temperature.

In the low-temperature (i.e. swollen) states, we further assume that $\phi_0 \ll 1$, so the leading-order balance of equation (2.17) is

$$\phi_0 \approx \left[\Omega\left(\frac{1}{2} - (A_0 - A_1) - (B_0 - B_1)T\right)\right]^{-3/5}, \tag{2.18}$$

equal to the classical approximation in gels that are not thermo-responsive (Doi 2009; Webber & Worster 2023). In both of the models, this gives $\phi_0 \sim 0.01$ for sufficiently low temperatures, but there is a singularity at

$$T = \frac{1 - 2(A_0 - A_1)}{2(B_0 - B_1)}, \tag{2.19}$$

where the assumption of small polymer fraction can no longer be applied, corresponding to approximately 308 K in the ANB model and 311 K in the HHT model. This is close to the measured critical temperatures at which the affinity for water molecules drops rapidly and the gel dries out, T_C (equal to around 305 K and 307.6 K in the two cases, respectively).

In the present study, we only wish to capture the rapid qualitative difference in the equilibrium polymer fraction $\phi_0(T)$ around some critical temperature T_C, and so we fit a simpler expression for $\phi_0(T)$ onto the full predictions of our model. To achieve this, we take

$$\phi_0(T) = \begin{cases} \phi_{00} & T < T_C \\ \phi_{0\infty} & T > T_C \end{cases}, \tag{2.20}$$

where $\phi_{00} = \phi_0(0)$ and $\phi_{0\infty} = \lim_{T\to\infty} \phi_0(T)$. Since we are not especially interested in the phenomena associated with the multivalued nature of $\phi_0(T)$ (and thus cases where $T_C^{\uparrow} \neq T_C^{\downarrow}$, we will use the Hirotsu *et al.* (1987) (HHT) parameters from now on, and can use MATLAB's lsqnonlin to fit the parameters†

$$\phi_{00} = 0.02552, \quad \phi_{0\infty} = 0.9944, \quad \text{and} \quad T_C = 307.9\,\text{K}. \tag{2.21}$$

2.3. *Linearised osmotic pressure*

We further make the simplifying assumption, as employed for example by Doi (2009) and Webber & Worster (2023), that the osmotic pressure is a linear function of ϕ at a fixed value of T, and thus that

$$\Pi(\phi, T) = \Pi_0(T)\,\frac{\phi - \phi_0(T)}{\phi_0(T)} \quad \text{with} \quad \Pi_0(T) = \phi_0(T)\left.\frac{\partial \Pi}{\partial \phi}\right|_{\phi=\phi_0(T)}. \tag{2.22}$$

This allows us to incorporate qualitative effects of temperature response without introducing an analytically-complicated model, and is equivalent to assuming that the polymer fraction is everywhere close to the local equilibrium value $\phi_0(T)$. From this starting point, we can also introduce an osmotic modulus $K(\phi, T)$ defined by

$$K(\phi, T) = \phi\frac{\partial \Pi}{\partial \phi} = \frac{\Pi_0(T)\phi}{\phi_0(T)}. \tag{2.23}$$

Using the simplified form of ϕ_0 introduced in equation (2.20), equations (2.22) and (2.23) become

$$\Pi(\phi, T) = \begin{cases} \Pi_{00}\dfrac{\phi - \phi_{00}}{\phi_{00}} & T < T_C \\ \Pi_{0\infty}\dfrac{\phi - \phi_{0\infty}}{\phi_{0\infty}} & T > T_C \end{cases} \quad \text{and} \quad K(\phi, T) = \begin{cases} \dfrac{\Pi_{00}\phi}{\phi_{00}} & T < T_C \\ \dfrac{\Pi_{0\infty}\phi}{\phi_{0\infty}} & T > T_C \end{cases}. \tag{2.24}$$

2.4. *Swelling and drying of gel spheres*

As a first example of the effect of changing the temperature on the composition of a hydrogel, consider a sphere of gel at equilibrium at some temperature $T \ll T_C$ in water. Within the bead of radius a_0, the polymer fraction will be a uniform ϕ_{00}. If the temperature is raised above T_C, as was investigated by Butler & Montenegro-Johnson (2022), the sphere will dry rapidly owing to osmotic effects, following the (spherically-symmetric) advection-diffusion equation of equation (2.7),

$$\frac{\partial \phi}{\partial t} + q_r\frac{\partial \phi}{\partial r} = \frac{1}{r^2}\frac{\partial}{\partial r}\left[r^2 D(\phi)\frac{\partial \phi}{\partial r}\right], \tag{2.25}$$

† The model parameters proposed by Afroze *et al.* (2000) (ANB) result in the fitting parameters $\phi_{00} = 0.03789$, $\phi_{0\infty} = 0.8099$ and $T_C = 305.8\,\text{K}$, but the multivalued equilibrium curve is clearly not captured here.

with $q_r \equiv 0$, since the phase-averaged flux is solenoidal and equal to zero at the origin. Conservation of polymer sets the evolution of the sphere radius, with

$$4\pi \int_0^{a(t)} r^2 \phi \, \mathrm{d}r = \frac{4\pi}{3} a_0^3 \phi_{00}, \tag{2.26}$$

which can be differentiated with respect to time, substituting from equation (2.25) for $\partial\phi/\partial t$ to find

$$\frac{\mathrm{d}a}{\mathrm{d}t} = -\left.\frac{D(\phi)}{\phi}\frac{\partial\phi}{\partial r}\right|_{r=a(t)}. \tag{2.27}$$

In order to validate our approach against Butler & Montenegro-Johnson (2022), we match model assumptions for the drying sphere case. Thus, we consider constant permeability k, take μ_s to have the form of equation (2.15*b*), and finally we relax the assumption of linear osmotic pressure (so as to better compare with the fully nonlinear results of other authors). These conditions imply that

$$D(\phi) = \frac{k k_B T}{\mu_l \Omega_f}\left\{\frac{\phi - \phi^{1/3}/3}{\Omega} + \frac{\phi^2}{1-\phi} + 2\phi^2\left[\chi + (1-2\phi)\frac{\partial\chi}{\partial\phi}\right] + \frac{4\phi^{1/3}}{3\Omega}\right\}. \tag{2.28}$$

The polymer fraction ϕ_1 at the gel–water interface $r = a(t)$ is set through taking continuity of pervadic pressure and normal stress. As in Webber & Worster (2023), this gives

$$\Pi(\phi_1) = 4\mu_s\left[\frac{a_0}{a(t)} - \left(\frac{\phi_1}{\phi_{00}}\right)^{1/3}\right]. \tag{2.29}$$

Making the scalings $\Phi = \phi/\phi_{00}$, $A = a/a_0$, $R = r/a_0$ and $\tau = k k_B T t/\mu_l \Omega_f a_0^2$, the non-dimensional diffusivity is

$$\mathcal{D} = \frac{\phi - \phi^{1/3}/3}{\Omega} + \frac{\phi^2}{1-\phi} + 2\phi^2\left[\chi + (1-2\phi)\frac{\partial\chi}{\partial\phi}\right] + \frac{4\phi^{1/3}}{3\Omega} \tag{2.30}$$

and the subsequent drying of the sphere is described by

$$\frac{\partial\Phi}{\partial\tau} = \frac{1}{R^2}\frac{\partial}{\partial R}\left[R^2\mathcal{D}(\Phi)\frac{\partial\Phi}{\partial R}\right] \quad \text{with} \quad \Phi(R,0) = 1,\ A(0) = 1,\ \left.\frac{\partial\Phi}{\partial R}\right|_{R=0} = 0, \tag{2.31a}$$

$$\frac{\phi_1 - \phi_1^{1/3}}{\Omega} - \phi_1 - \ln(1-\phi_1) - \phi_1^2\chi + \phi_1^2(1-\phi_1)\frac{\partial\chi}{\partial\phi} = \frac{4\phi_{00}^{1/3}}{3\Omega}\left[A^{-1} - \left(\frac{\phi_1}{\phi_{00}}\right)^{1/3}\right], \tag{2.31b}$$

$$\frac{\mathrm{d}A}{\mathrm{d}\tau} = -\left.\frac{\mathcal{D}(\Phi)}{\Phi}\frac{\partial\Phi}{\partial R}\right|_{R=A(\tau)}, \tag{2.31c}$$

where $\Phi(A,\tau) = \phi_1/\phi_{00}$. The Neumann boundary condition at $R = 0$ arises from no radial flow at the origin, whilst the final condition for $\mathrm{d}A/\mathrm{d}\tau$ is a non-dimensionalisation of equation (2.27).

In order to compare our model's predictions with those of the full nonlinear problem, we reproduce the swelling and drying problems of figures 8, 9 and 10 in Butler & Montenegro-Johnson (2022), where the temperature is varied around the critical temperature. Taking $\phi_{00} = \phi_0(304\,\mathrm{K})$, remark that

$$\phi_{00} = 5.227\times10^{-2} \quad \text{and} \quad \tau = \frac{\Omega\, t_{BMJ}}{\phi_{00}^{2/3}} = 100.7\, t_{BMJ}, \tag{2.32}$$

where t_{BMJ} is the dimensionless time used by Butler & Montenegro-Johnson (2022). The

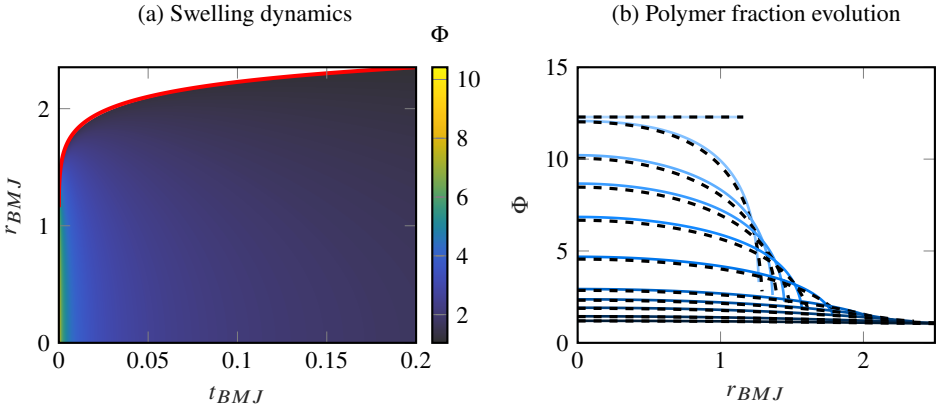

Figure 3: Plots illustrating the swelling of a hydrogel bead after the temperature is lowered from 308 K to 304 K at $\tau = 0$. The parameters used are the same as in Butler & Montenegro-Johnson (2022), with the fully nonlinear results plotted for comparison. On the left, the evolving polymer fraction is shown with the growth of the radius in the fully nonlinear model shown as a red curve. On the right, porosity profiles are shown at $t_{BMJ} = 0.0001, 0.0002, 0.0005, 0.001, 0.0025, 0.01, 0.05, 0.1, 0.2, 0.5$ and 1, with darker blue representing later times. Results from the fully nonlinear model are shown as dashed lines.

radial variable, r_{BMJ}, is scaled with the *dry* radius of the sphere, and is therefore given by $r_{BMJ} \approx 2.674R$.

We first compare the swelling behaviour of a gel with the HHT parameters that is initially in equilibrium at $T = 308\,\mathrm{K}$ before being rapidly brought into surroundings at temperature $T = 304\,\mathrm{K}$, swelling from an initial polymer fraction $\phi_0(308\,\mathrm{K}) = 0.6425$ to ϕ_{00} smoothly throughout. Figure 3 illustrates good quantitative and qualitative agreement with the results of Butler & Montenegro-Johnson (2022), with marginally slower growth of the radius but the same diffusive transport of water from the surroundings into the core of the gel. To understand any differences between the two models, we can recast the full nonlinear model in our variables, and compare expressions for $\mathcal{D}$ and the boundary conditions to find sources of discrepancy. In appendix B, we show that the rate of change of polymer fraction in time is lower in the LENS model than in the fully-nonlinear approach when $\partial\phi/\partial r < 0$, explaining why the approach to the steady swollen state is slightly slower in our model than that seen by Butler & Montenegro-Johnson (2022).

Repeating this analysis for the drying of a bead, we consider the case of smooth drying where there is no formation of a drying front (a feature that we will discuss in more depth below). Raising the temperature from $T = 304\,\mathrm{K}$ to $307.6\,\mathrm{K}$, the plots in figure 4 illustrate good agreement with the fully-nonlinear solution, but faster drying in the LENS approach. Again, this can be expected from considering the analysis in appendix B, with faster polymer fraction evolution for drying, and an altogether similar interfacial polymer fraction between the two models at $T = 307.6\,\mathrm{K}$. There is a more significant discrepancy between the predictions of LENS and the fully-nonlinear model in this case owing to the larger polymer fraction gradients present at around $t_{BMJ} = 5$. Importantly, this model also captures the particular drying trajectory featuring fast drying at early times and between $t_{BMJ} = 5$ and $t_{BMJ} = 6$, and slow drying in a plateau region $2 \leqslant t_{BMJ} \leqslant 5$. This occurs since the solution approaches regions of parameter space where we may expect phase separation, and the presence of a nearby equilibrium solution gives a critical slow-down behaviour akin to that discussed by Gomez *et al.* (2017).

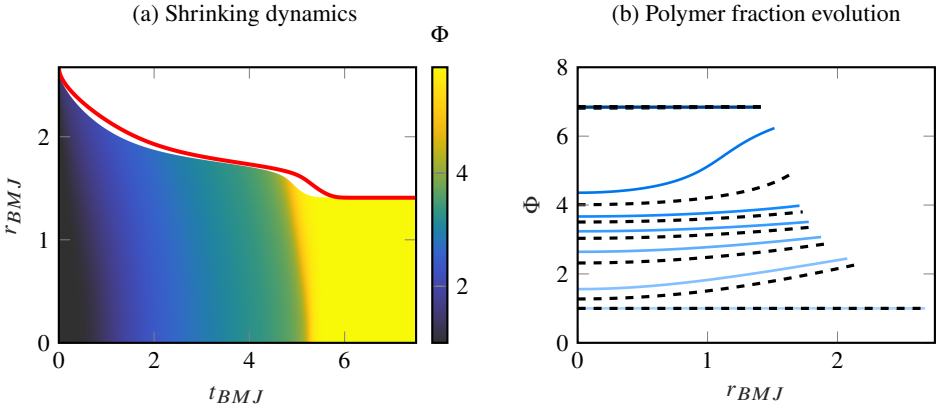

Figure 4: Plots illustrating the drying of a hydrogel bead after the temperature is raised from 304 K to 307.6 K at $\tau = 0$, with the HHT parameters as before and the fully nonlinear solution plotted for comparison. On the left, the evolving porosity is shown with the growth of the radius in the fully nonlinear model shown as a red curve. On the right, porosity profiles are shown at $t_{BMJ} = 0, 1, 2, 3, 4, 5, 6, 7$ and 8, with darker blue representing later times. Results from the fully nonlinear model are shown as dashed lines.

This phase separation, where shrunken and swollen states can locally coexist with a sharp front in between, is one of the key phenomena investigated by Butler & Montenegro-Johnson (2022). Often during the deswelling process a sharp drying front forms, travelling radially inwards through the bead, with the exterior rapidly drying to its final state and the interior remaining relatively swollen until the front reaches the centre. This occurs when trajectories in (T, ϕ)-space pass through the spinodal or coexistence regions. In the spinodal region, spontaneous phase separation can occur, with the formation of regions of dried polymer surrounded by swollen gel or vice versa as the system equilibrates. The coexistence region is a special case of this, where a dried gel and a swollen one can coexist in thermodynamic equilibrium with a simple sharp boundary (such as a drying front) separating the two. In the present study, we consider both of these effects to be forms of spinodal decomposition, with coexistence a weaker 'local' form. In either case, there are sharp differences in ϕ across very short distances.

Since large gradients in polymer fraction lead to large deviatoric strains, we expect that our model is unlikely to capture the dynamics of these sharp fronts exactly, since it is dependent on the assumption that these strains remain small. Attempting to replicate this behaviour regardless, through raising the temperature from 304 K to 308 K, shows that the polymer diffusivity is, in fact, negative for such a case in our model. This leads to spinodal decomposition, with $D(\phi) < 0$, i.e.

$$\frac{\phi - \phi^{1/3}/3}{\Omega} + \frac{\phi^2}{1-\phi} + 2\phi^2\left[\chi + (1-2\phi)\frac{\partial \chi}{\partial \phi}\right] + \frac{4\phi^{1/3}}{3\Omega} < 0 \tag{2.33}$$

the criterion for such behaviour to occur. Figure 5 shows the trajectory of swelling and drying problems in (T, ϕ)-space, making it clear why swelling (when the temperature is lowered) never leads to negative diffusivities, and why some drying can occur (such as that of figure 4) without entering the spinodal region. In the remainder of this paper, we will consider cases of smooth drying where phase separation does not occur.

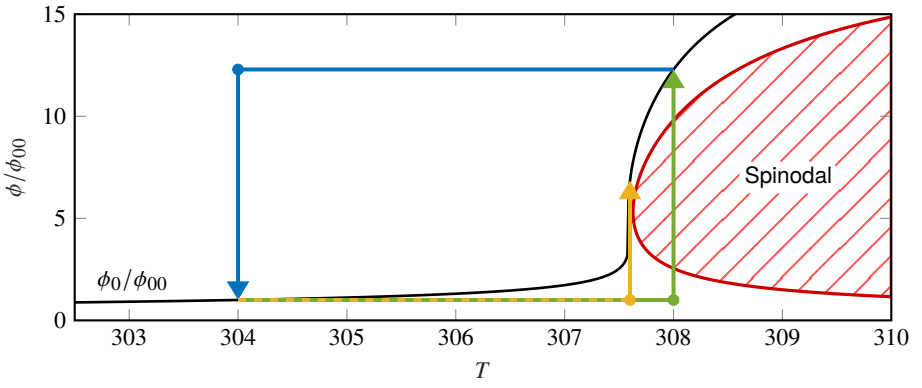

Figure 5: A plot of the region in $(T,\ \phi)$-space where the polymer diffusivity is negative (spinodal region), alongside the equilibrium polymer fraction $\phi_0(T)$. The smooth swelling problem of figure 3 is plotted in blue, with the temperature lowered and the spinodal region never approached, and the smooth drying of figure 4 is plotted in yellow. Phase separation occurs when the temperature is raised to 308 K and the path to equilibrium passes through the spinodal region, as shown in the example green trajectory.

3. Response times and flow in thermo-responsive tubes

The analysis presented in section 2.4 illustrates how the response time for a gel to a change in the local temperature is set by the poroelastic timescale for the gel. In the plots of figure 3, we see that a swelling sphere only attains its final radius at a time $O(\mu_l a_0^2/k\Pi_{0\infty})$ after the temperature has been changed. In general, these timescales are slow, of the order of many hours for most macroscopic gels of interest (Webber & Worster 2023), since the response is rate-limited by the permeability k, typically of the order 10^{-15} m^2 or smaller (Etzold *et al.* 2021).

In general, scaling the terms in equation (2.7) shows that the poroelastic timescale t_{pore} is given in an arbitrary geometry by

$$t_{\text{pore}} \sim \frac{\mu_l L^2}{k\Pi_{0\infty}}, \tag{3.1}$$

where L is a lengthscale for the problem. If the physical situation we are modelling has a fixed size L, we seek an approach to lower the poroelastic timescale for fixed L so that the gel reacts more quickly. Recently, a new class of microfluidic actuators have been designed, reliant on simple geometric designs to convert the isotropic shrinkage of hydrogels above the LCST threshold into more complicated anisotropic morphological changes (Maslen *et al.* 2023). Even at the micrometre-scale, these devices take a number of seconds to pass through a single actuation cycle, and with deswelling times scaling like L^2, centimetre- or millimetre-scale devices harnessing the same physics can be expected to take many hours to achieve the same shape changes. This currently confines such applications to microfluidics, whilst an approach that lowers the response times could find applications in actuators or soft robotics on the macroscopic scale.

Concurrently, a number of recent advances in microfluidics have harnessed the ability of hydrogels to pump fluid, either passively through their hydrophilic nature (Dong & Jiang 2007), or through the use of responsive hydrogels to drive peristaltic flows (Richter *et al.* 2009). In this latter case, fluid flows many orders of magnitude faster than the percolating flow through the gel matrix can be achieved by squeezing water through microscale voids in the structure.

In this section, we consider the simple case of a tube of thermo-responsive hydrogel

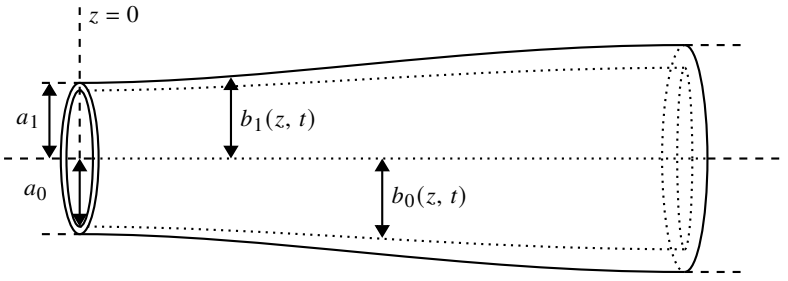

Figure 6: A diagram illustrating the tube of hydrogel in the space $b_0 < r < b_1$ with a hollow lumen inside. Note that $b_1 = a_1$ and $b_0 = a_0$ at $z = 0$, and symmetry at this point implies that we need only solve the problem in $0 < z < \infty$.

surrounded by (and filled with) bulk water, occupying the region $a_0 < r < a_1$ when $T < T_C$, with uniform polymer fraction ϕ_{00}. When the temperature is brought above the critical value, the gel will dry, leading to a shrinkage of the tube, and the expulsion of water. This water can be expelled radially out of the tube, carried (slowly) through the gel parallel to the axis, or can be transported axially in the lumen of the tube. Though the deswelling response to the temperature change is still governed by the poroelastic timescale, the tube can be manufactured to be sufficiently thin that shrinkage is rapid, and bulk water can be transported much more rapidly through the hollow lumen than would otherwise be the case for a solid cylinder (as in the case investigated by Webber *et al.* (2023)), such that the gel device acts like a small-scale displacement pump, reacting on a much faster timescale.

3.1. *Model problem*

Consider an infinite tube formed from thermo-responsive gel, with an initial thickness $a_1 - a_0$. Initially, the temperature is $T_C - \Delta T$, but for $t \geqslant 0$ a temperature $T = T_C + \Delta T$ is imposed at $z = 0$, and the tube deswells as the heat pulse spreads out diffusively in time. We make the simplifying assumption that the thermal properties of water and hydrogel are sufficiently similar, and that any flows are negligible from a thermodynamic point of view such that all heat transfer is diffusive, and restrict our attention to $z \geqslant 0$ by symmetry around $z = 0$. Then, the temperature field satisfies

$$\frac{\partial T}{\partial t} = \kappa \frac{\partial^2 T}{\partial z^2} \quad \text{with} \quad T(0, t) = T_C + \Delta T \quad \text{and} \quad \frac{\partial T}{\partial z} \to 0 \quad \text{as } z \to \infty, \tag{3.2}$$

for κ the thermal diffusivity. The second boundary condition arises from the assumption of no heat flux at infinity. Equation (3.2) has a solution in terms of the error function, with

$$T - T_C = \Delta T \left[2 \operatorname{erfc}\left(\frac{z}{2\sqrt{\kappa t}} \right) - 1 \right], \tag{3.3}$$

where erfc is the complementary error function (Abramowitz & Stegun 1970). In response to the change in temperature, water is expelled from the hydrogel and the shape of the tube is described by $b_0(z, t) < r < b_1(z, t)$, as illustrated in figure 6. In order to simplify the analysis that follows, we assume that there is no spinodal decomposition and that the osmotic pressure can be accurately described by the linear form of equation (2.24), for polymer fractions that remain close to $\phi_0(T)$ throughout. There is no consensus on the exact form that $\Pi(\phi)$ should take, with some recent research suggesting that a power-law dependence on polymer fraction (at least for the mixing contribution) leads to better agreement with experimental measurements than classical Flory-Huggins theory (Feng *et al.* 2024). Appendix

C compares some results from Butler & Montenegro-Johnson (2022) with those obtained using a linearised osmotic pressure, showing good qualitative, if not quantitative, agreement. While, all of the following analysis could be repeated with more complicated expressions for $\Pi(\phi)$, if necessary, we have opted for the simpler form to facilitate analytical insight.

3.1.1. *Deformation of the tube*

As a first model, assume that all deformation is locally isotropic, and that deswelling leads to a displacement field (relative to the initial state) with axial component η and radial component ξ given by

$$\frac{\xi}{r} \approx \frac{\partial \xi}{\partial r} \approx \frac{\partial \eta}{\partial z} \approx 1 - \left(\frac{\phi}{\phi_{00}}\right)^{1/3}. \tag{3.4}$$

Making this assumption requires the polymer fraction field to be independent of r at leading order, an assumption that is reasonable to make in the slender limit of a tube with much larger horizontal lengthscale than diameter. Since we expect $\xi = 0$ at $r = 0$ (in the limit of no lumen) and $\eta = 0$ at $z = 0$, the leading-order displacement field is

$$\xi = \left[1 - \left(\frac{\phi}{\phi_{00}}\right)^{1/3}\right] r \quad \text{and} \quad \eta = \int_0^z \left[1 - \left(\frac{\phi}{\phi_{00}}\right)^{1/3}\right] \mathrm{d}u. \tag{3.5}$$

Using the expression above for ξ allows us to write

$$\frac{b_0}{a_0} \approx \frac{b_1}{a_1} \approx \left(\frac{\phi}{\phi_{00}}\right)^{-1/3}, \tag{3.6}$$

and so the local thickness of the tube is proportional to $\phi^{-1/3}$. In order to quantify this deformation as a result of deswelling, we must first understand how the polymer fraction changes in response to temperature changes.

3.1.2. *Polymer fraction evolution*

To describe the evolution of polymer fraction in time as the gel expels water, equation (2.7) becomes

$$\frac{\partial \phi}{\partial t} + \boldsymbol{q} \cdot \boldsymbol{\nabla} \phi = \frac{1}{r}\frac{\partial}{\partial r}\left[rD(\phi, T)\frac{\partial \phi}{\partial r}\right] + \frac{\partial}{\partial z}\left[D(\phi, T)\frac{\partial \phi}{\partial z}\right] \quad \text{with}$$

$$D(\phi, T) = \frac{k}{\mu_l}\left[\frac{\Pi_0(T)\phi}{\phi_0(T)} + \frac{4\mu_s}{3}\left(\frac{\phi}{\phi_{00}}\right)^{1/3}\right], \tag{3.7}$$

again making the assumption of constant permeability and shear modulus. In order to simplify the analysis, we make a slenderness assumption that the characteristic axial lengthscale L is much greater than the characteristic radial lengthscale a_1. Define $\varepsilon = a_1/L$, and assume that the polymer fraction field only has leading-order axial variation, with radial differences in polymer fraction being of the order $\delta \ll 1$ (arising from our assumption of local isotropy),

$$\phi = \phi_1(z, t) + \delta\phi_2(r, z, t). \tag{3.8}$$

We define ϕ_1 to be the polymer fraction on $r = b_0(z, t)$ with ϕ_2 the radial structure function equal to zero on $r = b_0$. Plugging this into the evolution equation above allows us to separate variables and deduce that $\delta = \varepsilon^2$. Therefore, we need only make a relatively weak slenderness assumption, since it is ε^2 that must be small and not ε itself, making this model applicable for relatively stout tubes.

If we let $Z = z/L$ and $R = r/a_1$, the leading-order balance of equation (3.7) is

$$L^2\frac{\partial\phi_1}{\partial t} + Lq_z\frac{\partial\phi_1}{\partial Z} = \frac{1}{R}\frac{\partial}{\partial R}\left[RD(\phi_1,T)\frac{\partial\phi_2}{\partial R}\right] + \frac{\partial}{\partial Z}\left[D(\phi_1,T)\frac{\partial\phi_1}{\partial Z}\right], \tag{3.9}$$

since the material flux $\boldsymbol{q} = q_r\hat{\boldsymbol{r}} + q_z\hat{\boldsymbol{z}}$ is solenoidal and thus $q_r/a_1 \sim q_z/L$. This motivates a non-dimensionalisation,

$$B_0 = \frac{b_0}{a_1},\ B_1 = \frac{b_1}{a_1},\ \tau = \frac{k\Pi_{00}t}{\mu_l L^2},\ Q = \frac{\mu_l L q_z}{k\Pi_{00}},\ \Phi_{1,2,\infty} = \frac{\phi_{1,2,0\infty}}{\phi_{00}},\ \mathcal{M} = \frac{\mu_s}{\Pi_{00}}. \tag{3.10}$$

We also define a non-dimensional diffusivity, arising from the linear osmotic pressure (2.24),

$$\mathcal{D}(\Phi_1, T) = \begin{cases} \Phi_1 + \dfrac{4\mathcal{M}}{3}\Phi_1^{1/3} & T < T_C \\ \dfrac{\Pi_{0\infty}}{\Pi_{00}}\dfrac{\Phi_1}{\Phi_\infty} + \dfrac{4\mathcal{M}}{3}\Phi_1^{1/3} & T > T_C \end{cases}. \tag{3.11}$$

Then, finally, the evolution equation governing the tube is

$$\frac{\partial\Phi_1}{\partial\tau} + Q\frac{\partial\Phi_1}{\partial Z} = \frac{1}{R}\frac{\partial}{\partial R}\left[R\mathcal{D}(\Phi_1,T)\frac{\partial\Phi_2}{\partial R}\right] + \frac{\partial}{\partial Z}\left[\mathcal{D}(\Phi_1,T)\frac{\partial\Phi_1}{\partial Z}\right], \tag{3.12}$$

to be solved subject to $\Phi_1 \equiv 1$ at $\tau = 0$, $\partial\Phi_1/\partial Z = 0$ at $Z = 0$ (by symmetry) and $\partial\Phi_1/\partial Z \to 0$ as $Z \to \infty$. Using equations (2.8) and (3.5), we find the non-dimensional flux to be

$$\begin{aligned} Q &= \frac{\mathcal{D}(\Phi_1,T)}{\Phi_1}\frac{\partial\Phi_1}{\partial Z} + \Phi_1^{-1/3}\frac{\partial(\eta/L)}{\partial\tau} \\ &= \frac{\mathcal{D}(\Phi_1,T)}{\Phi_1}\frac{\partial\Phi_1}{\partial Z} - \frac{\Phi_1^{-1/3}}{3}\int_0^Z \Phi_1^{-2/3}\frac{\partial\Phi_1}{\partial\tau}\,\mathrm{d}u. \end{aligned} \tag{3.13}$$

3.1.3. *Radial structure of the tube*

Separating variables for Φ_2 in the partial differential equation (3.12),

$$\frac{1}{R}\frac{\partial}{\partial R}\left[R\mathcal{D}(\Phi_1,T)\frac{\partial\Phi_2}{\partial R}\right] = f(Z,T,\tau), \tag{3.14}$$

with $\Phi_2 = 0$ on $R = B_0 = (a_0/a_1)\Phi_1^{-1/3}$ by definition. Hence,

$$\Phi_2 = \frac{f(Z,T,\tau)R^2}{4\mathcal{D}(\Phi_1,T)} + g(Z,T,\tau)\log R + h(Z,T,\tau). \tag{3.15}$$

Without loss of generality, we can absorb the term h into Φ_1, since it does not depend on R, and determine g from boundary conditions at the inner tube–water interface $R = B_0$, where $\Phi_2 = 0$. Letting a_0/a_1 be denoted by $\ell < 1$, $B_0 = \ell\Phi_1^{-1/3}$ and

$$\Phi_2 = \frac{f(Z,T,\tau)}{4\mathcal{D}(\Phi_1,T)}\left[R^2 - \frac{\ell^2\Phi_1^{-2/3}}{\log\ell - (\log\Phi_1)/3}\log R\right]. \tag{3.16}$$

At the outermost interface $R = B_1$, the pervadic pressure is taken, without loss of generality, to be zero, since this quantity is continuous across the material boundary. Requiring no radial stress here ($\sigma_{rr} = 0$) therefore reduces to requiring that osmotic pressures are balanced by

shear, and

$$\Pi(\phi_1 + \varepsilon^2\phi_2) = 2\mu_s\left[\frac{\partial\xi}{\partial r} - 1 + \left(\frac{\phi}{\phi_{00}}\right)^{1/3}\right] = 0. \tag{3.17}$$

This imposes $\Phi = \Phi_0(T)$ on $R = B_1$, or that the polymer fraction here equals the equilibrium value. Therefore,

$$f(Z, T, \tau) = \frac{4\Phi_1^{2/3}\mathcal{D}(\Phi_1, T)}{\varepsilon^2}\frac{3\log\ell - \log\Phi_1}{3\log\ell - (1-\ell^2)\log\Phi_1}\left[\Phi_0(T) - \Phi_1\right], \tag{3.18}$$

implying that, for our model to be consistent, Φ_1 must everywhere be close to the piecewise-constant equilibrium polymer fraction Φ_0, or else our scaling arguments for the terms in the advection-diffusion equation will be invalid. We can check this assumption after calculating the solution to verify the validity of our modelling.

3.1.4. *Model summary*

In order to understand the response of the gel to the diffusive heat pulse, we first seek the position of the drying front $z = z_C$ where $T = T_C$. This is found using equation (3.3), with

$$\operatorname{erfc}\left(\frac{z_C}{2\sqrt{\kappa t}}\right) = \frac{1}{2} \quad \text{so} \quad z_C = 2\operatorname{erfc}^{-1}\left(\frac{1}{2}\right)\sqrt{\kappa t} \approx 0.9539\sqrt{\kappa t}. \tag{3.19}$$

We introduce a Lewis number, the ratio of thermal to compositional diffusivities, defined by $Le = \mu_l\kappa/k\Pi_{00}$, such that this drying front can now be described in non-dimensional variables,

$$Z_C(\tau) = 2\sqrt{Le}\operatorname{erfc}^{-1}\left(\frac{1}{2}\right)\tau^{1/2}. \tag{3.20}$$

Then,

$$\frac{\partial\Phi_1}{\partial\tau} + \frac{\mathcal{D}}{\Phi_1}\left(\frac{\partial\Phi_1}{\partial Z}\right)^2 - \frac{\Phi_1^{-1/3}}{3}\frac{\partial\Phi_1}{\partial Z}\int_0^Z \Phi_1^{-2/3}\frac{\partial\Phi_1}{\partial\tau}\,\mathrm{d}u = f + \frac{\partial}{\partial Z}\left[\mathcal{D}\frac{\partial\Phi_1}{\partial Z}\right] \quad \text{with}$$

$$\mathcal{D} = \begin{cases} \tilde{\Pi}\dfrac{\Phi_1}{\Phi_\infty} + \dfrac{4\mathcal{M}}{3}\Phi_1^{1/3} & Z < Z_C \\ \Phi_1 + \dfrac{4\mathcal{M}}{3}\Phi_1^{1/3} & Z > Z_C \end{cases} \quad \text{and}$$

$$f = \frac{4\Phi_1^{2/3}\mathcal{D}}{\varepsilon^2}\frac{3\log\ell - \log\Phi_1}{3\log\ell - (1-\ell^2)\log\Phi_1} \times \begin{cases} \Phi_\infty - \Phi_1 & Z < Z_C \\ 1 - \Phi_1 & Z > Z_C \end{cases}. \tag{3.21}$$

Here, $\tilde{\Pi}$ represents $\Pi_{0\infty}/\Pi_{00}$. This is to be solved with the initial conditions $\Phi_1 \equiv 1$ and subject to boundary conditions $\partial\Phi_1/\partial Z = 0$ at $Z = 0$ and $\partial\Phi_1/\partial Z \to 0$ as $Z \to \infty$. From this solution, the shape of the gel can be deduced,

$$\ell\Phi_1^{-1/3} \leqslant R \leqslant \Phi_1^{-1/3}, \tag{3.22}$$

as well as the radial polymer fraction structure using equation (3.16).

3.2. *Response to uniform temperature change*

Before studying the response of a hollow tube to a propagating heat pulse, we first consider the case where the temperature is everywhere brought up to $T_C + \Delta T$. The response of the

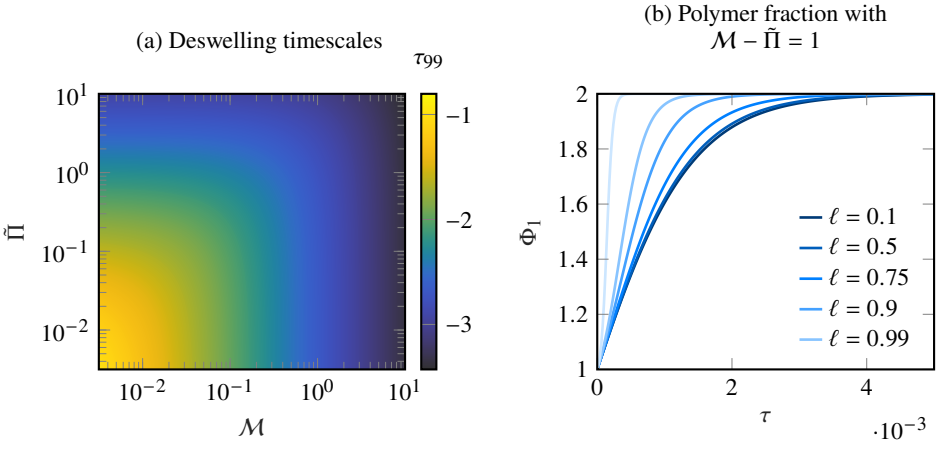

Figure 7: Plots of the one-dimensional deswelling of a tube when the temperature is uniformly changed when $\Phi_\infty = 2$ and $\varepsilon = 0.1$. This shows the variation of the deswelling timescale τ_{99} (the time taken for $\Phi_1 \geqslant 1.99$) and the approach to steady state for a number of tube thicknesses.

tube is axially-uniform, evolving following a simplified form of equation (3.21),

$$\frac{\partial \Phi_1}{\partial \tau} = \frac{4(\Phi_\infty - \Phi_1)}{\varepsilon^2} \frac{3\log \ell - \log \Phi_1}{3\log \ell - (1-\ell^2)\log \Phi_1} \left(\tilde{\Pi} \frac{\Phi_1^{1/3}}{\Phi_\infty} + \frac{4\mathcal{M}}{3} \Phi_1 \right). \tag{3.23}$$

We can use this equation to understand how the material parameters Φ_∞, $\mathcal{M}$ and $\tilde{\Pi}$ affect the response time to a change in temperature without the added complication of spatial variations. We know that the polymer fraction on the inside of the tube will approach Φ_∞ as time goes on, with the outside polymer fraction instantaneously reaching this value, but the rate at which this steady state is approached may vary. To measure the rate of deswelling, define the deswelling timescale τ_{99} as the time taken for

$$\Phi_1 \geqslant \Phi^* - \frac{\Phi^* - 1}{100}. \tag{3.24}$$

Straightforwardly, it is clear that deswelling is more rapid when there is a greater contrast between ϕ_{00} and $\phi_{0\infty}$, since the bracketed term $\Phi_\infty - \Phi_1$ is greater in magnitude. Thus, gels with more dramatic deswelling will reach their steady states faster. Figure 7a shows how the time taken to reach Φ_∞ depends on the stiffness of the gel (encoded by $\mathcal{M}$) and the strength of the osmotic pressure at higher temperatures (encoded by $\tilde{\Pi}$). Stiffer gels resist the formation of deviatoric strains, which arise from differences in polymer fraction, so the interior must deswell to catch up with the outside of the tube, leading to a much faster deswelling process as $\mathcal{M}$ increases. Similarly, larger values of $\tilde{\Pi}$ lead to more rapid interstitial flows driven by pervadic pressure gradients, and so the time to deswell decreases as $\tilde{\Pi}$ increases.

Figure 7b illustrates the approach of the polymer fraction on the interior of the tube to the equilibrium value Φ_∞, showing how the approach is more rapid for thinner tubes where there is a shorter distance for water to diffuse out. Even though the initial rate of drying is independent of ℓ (at $\tau = 0$), at later times, drying is more rapid when $\ell \to 1$. Henceforth, we will use the parameter values of table 2 in all calculations unless otherwise specified, and only investigate the effect of varying tube thickness through ℓ.

Parameter	Value
Deswollen scaled polymer fraction Φ_∞	2
Ratio of osmotic pressure scales $\tilde{\Pi}$	1
Aspect ratio $\varepsilon = a_1/L$	0.1
Shear parameter $\mathcal{M}$	1
Lewis number Le	10

Table 2: Parameter values used in the modelling of drying tubes from section 3.3 onwards, with the effect of changing Φ_∞, $\tilde{\Pi}$ and $\mathcal{M}$ discussed in section 3.2.

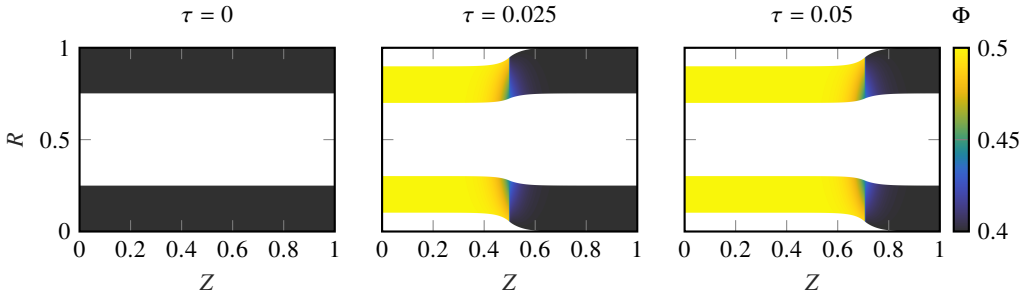

Figure 8: Plots of the evolution of a hollow thermo-responsive hydrogel tube with parameters from table 2 and $\ell = 0.5$. The heat pulse diffuses from left to right, with the gel shrinking behind it.

3.3. *Flow response to heat pulses*

Using the model summarised in equation (3.21), we can compute the mechanisms by which a thermo-responsive gel tube will collapse in response to a heat pulse starting at $Z = 0$. Key to the behaviour here is the fact that heat diffuses on a faster timescale than the water can diffuse through the polymer, leading to a smooth front centred on the heat pulse. This corresponds to the $Le \gg 1$ limit – using the approximate value $\Pi_{00} \sim 10^4$ Pa (Webber & Worster 2023) and $k \sim 10^{-15}\,\mathrm{m}^2$ (Etzold *et al.* 2021), it is found that $Le \sim 10$ and the heat pulse is transported an order of magnitude faster than water through the pores. Figure 8 shows the thickness of a tube at different times as heat diffuses and the gel shrinks. Notice that the shrinkage, though rapid, is not instantaneous in time, since the slow diffusion of water out of the walls of the tube sets a delayed response.

In order for the gel to deswell, water must flow from the walls of the tube into the surrounding water, the lumen at the centre of the tube, or through the gel itself parallel to the axis. Clearly, if the walls of the tube are thinner, driving water from the hydrogel is more rapid, since the water has less of a distance to diffuse outwards, and we expect a more rapid response to changes in temperature for larger values of ℓ. The more rapid approach to steady state is shown in figure 9a, where the sharper equilibrium profile is approached more closely around the drying front $Z_C(\tau)$ for thinner tube walls. Assuming that the radial fluxes are locally dominant, equation (3.21) reduces to the one-dimensional case of section 3.2,

$$\frac{\partial \Phi_1}{\partial \tau} \approx \frac{4\Phi_1^{2/3}\mathcal{D}}{\varepsilon^2} \frac{3\log\ell - \log\Phi_1}{3\log\ell - (1-\ell^2)\log\Phi_1} \times \begin{cases} \Phi_\infty - \Phi_1 & Z < Z_C \\ 1 - \Phi_1 & Z > Z_C \end{cases}, \tag{3.25}$$

(a) Relaxation to the equilibrium polymer fraction around Z_C

(b) Fitted values of $A(\ell)$ showing that $A \sim (1-\ell)^{-1/2}$

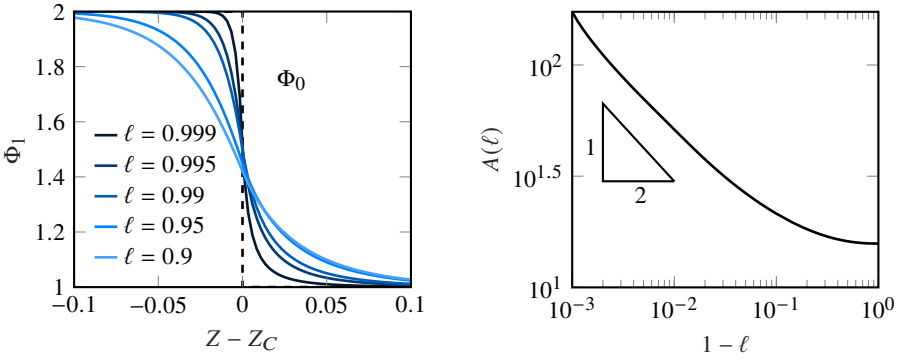

Figure 9: Plots of the interior polymer fraction Φ_1 at $\tau = 10^{-2}$ with the same parameters as in figure 8, showing how the relaxation to the steady state $\Phi = \Phi_0(T)$ around the drying front $Z = Z_C(\tau)$ is much faster for thinner tubes $\ell \to 1$. These profiles can be approximated by a tanh function, as in equation (3.27), with fitting parameter $A(\ell)$ shown in the logarithmic plot on the right.

away from the front at $Z = Z_C$ (where $\partial\Phi_1/\partial Z$ will be significant). Then, as $\ell \to 1$,

$$\frac{\partial \Phi_1}{\partial \tau} \to \frac{4\Phi_1^{2/3}\mathcal{D}}{\varepsilon^2(1-\ell)}\frac{\log\Phi_1}{3+2\log\Phi_1} \times \begin{cases} \Phi_\infty - \Phi_1 & Z < Z_C \\ 1 - \Phi_1 & Z > Z_C \end{cases}, \tag{3.26}$$

and timescales decrease like $1-\ell$. In the opposite limit as $\ell \to 0$, adjustment happens on the unmodified poroelastic timescale.

From figure 8, it is clear that the structure of the solution around $Z = Z_C(\tau)$ appears to propagate like a travelling wave centred on the deswelling front, since the contribution of axial flows through the gel is limited compared to that of radial flows. Therefore, we can consider the quasi-one-dimensional probelm in the new coordinate $Z - Z_C$. The plots in figure 9 suggest that polymer fraction can locally be approximated by a smooth step around $Z = Z_C(\tau)$, with the steepness a function of thickness ℓ. We thus propose that

$$\Phi_1 \approx \Phi_\infty - \frac{\Phi_\infty - 1}{2}\left\{1 + \tanh\left[A(\ell)\,(Z - Z_C)\right]\right\}, \tag{3.27}$$

for some scaling factor A, a function of ℓ, representing the sharpness of the drying front. Figure 9 shows that $A(\ell) \sim (1-\ell)^{-1/2}$, and therefore the thickness of the adjustment region around the front $Z = Z_C(\tau)$ scales like $(1-\ell)^{1/2}$.

3.3.1. *Flow through the walls*

Flow in the walls of the tube is driven by diffusive transport of water from more swollen regions to drier regions, with an interstitial fluid velocity

$$\boldsymbol{u_g} = \frac{D(\phi)}{\phi}\boldsymbol{\nabla}\phi = \frac{k\Pi_{00}}{\mu_l}\left(\frac{1}{L}\frac{\partial\Phi_1}{\partial Z}\hat{\boldsymbol{z}} + \frac{\varepsilon^2}{a_1}\frac{\partial\Phi_2}{\partial R}\hat{\boldsymbol{r}}\right) \times \begin{cases} \tilde{\Pi} + \dfrac{4\mathcal{M}}{3}\Phi_1^{-2/3} & Z < Z_C \\ 1 + \dfrac{4\mathcal{M}}{3}\Phi_1^{-2/3} & Z > Z_C \end{cases}, \tag{3.28}$$

at leading order in the aspect ratio. We define a dimensionless radial fluid velocity U_g scaled with a_1 divided by the poroelastic timescale and an axial velocity V_g scaled with L divided

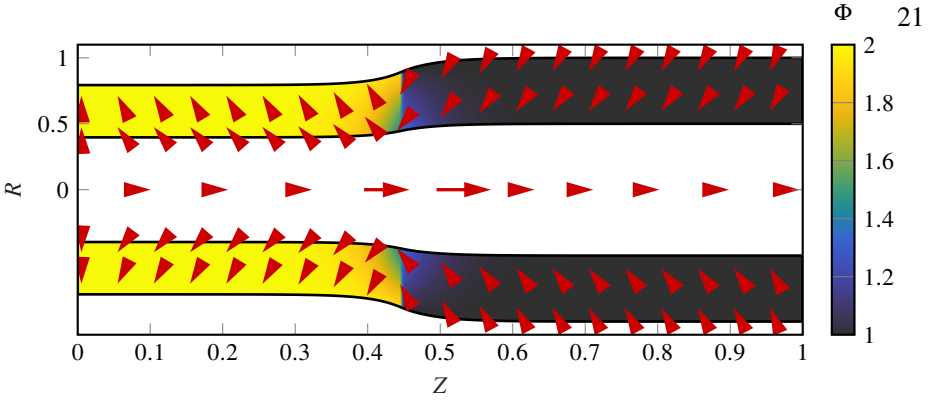

Figure 10: A plot at $\tau = 0.02$ of a drying gel tube with the same parameters as in figure 8. The colours represent the polymer fraction field, with arrows in the gel showing the direction and magnitude of the interstitial flow field $\boldsymbol{u_g}$, as defined in equation (3.28). The arrows along the centreline show the local magnitude of the parallel flow in the lumen, V, derived from equation (3.32).

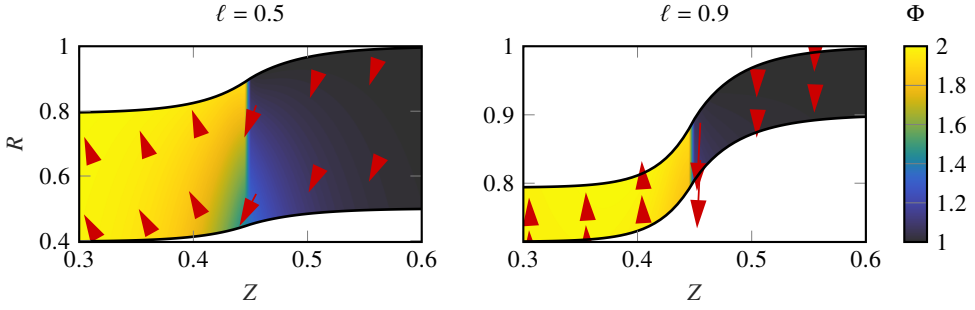

Figure 11: Plots close to $Z = Z_C(\tau)$ when $\tau = 0.02$, illustrating dominant radial flows when the gel is thinner ($\ell = 0.9$) versus the thicker ($\ell = 0.5$) gel. In all other regards, the parameters are the same as in figure 10. Notice the directional change either side of the drying front.

by the same timescale, so that

$$(V_g,\, U_g) = \left(\frac{\partial \Phi_1}{\partial Z},\, \frac{\partial \Phi_2}{\partial R}\right) \times \begin{cases} \tilde{\Pi} + \dfrac{4\mathcal{M}}{3}\Phi_1^{-2/3} & Z < Z_C. \\ 1 + \dfrac{4\mathcal{M}}{3}\Phi_1^{-2/3} & Z > Z_C. \end{cases} \tag{3.29}$$

Figure 10 illustrates an example flow field through the walls of the gel, with flow from more swollen to less swollen regions. In the dried region behind the temperature front, radial fluxes are outwards as water is driven out of the shrinking gel, with fluid transported axially towards the drier regions to the left. In $Z > Z_C$, however, fluxes are radially inwards. In order to understand why this is, notice that the gel is more swollen on its interior than exterior when $Z < Z_C$ (as the tube fully dries from the outside in) and more swollen on its exterior than interior when $Z > Z_C$ (as the tube is fully swollen on $R = B_1$ with some loss of fluid in the interior due to axial fluxes towards the drier tube). Hence, there needs to be water drawn in from the surrounding fluid to replenish these regions.

In general, therefore, the tube draws water inwards ahead of the deswelling front, and then expels the water behind this front. This is shown in detail in figure 11, where the dominance of radial fluxes in thinner gel layers is also clear.

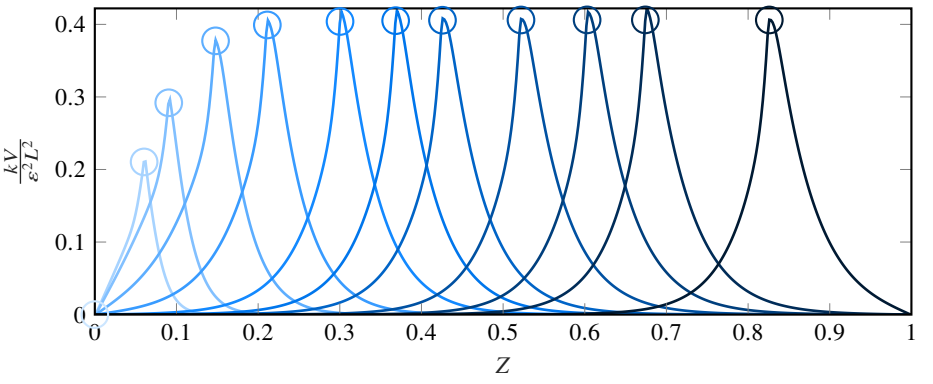

Figure 12: Plots of the lumen flux V as time progresses with $\ell = 0.5$. Circles mark $Z_C(\tau)$ and earlier times are lighter colours.

3.3.2. *Flow in the lumen*

There is also transport of water in the lumen within the tube, which is much faster than the slow diffusion through the tube walls. Assuming that this transport occurs at a non-dimensional velocity V (scaled with L divided by the poroelastic timescale) parallel to the axis, we treat the flow through the pipe as cylindrical Poiseuille flow driven by gradients in the pervadic pressure. Imposing a zero radial stress condition at $R = B_0$, much as when seeking the interfacial boundary condition at $R = B_1$ in equation (3.17),

$$p + \Pi(\phi_1) = 0 \quad \text{so} \quad \frac{p}{\Pi_{00}} = \begin{cases} \tilde{\Pi}\left(\Phi^* - \Phi_1\right) & Z < Z_C(\tau) \\ 1 - \Phi_1 & Z > Z_C(\tau) \end{cases}, \tag{3.30}$$

driving a flow from left to right with the heat pulse, with a dimensional average velocity (via the standard Hagen-Poiseuille flow law) in the tube lumen given by

$$-\frac{\Pi_{00} a_1^2 \ell^2 \Phi_1^{-2/3}}{8\mu_l L} \frac{\partial \Phi_1}{\partial Z} \times \begin{cases} \tilde{\Pi} & Z < Z_C(\tau) \\ 1 & Z > Z_C(\tau) \end{cases}. \tag{3.31}$$

Non-dimensionalising,

$$V = -\frac{\varepsilon^2 L^2}{k} \frac{\ell^2 \Phi_1^{-2/3}}{8} \frac{\partial \Phi_1}{\partial Z} \times \begin{cases} \tilde{\Pi} & Z < Z_C(\tau) \\ 1 & Z > Z_C(\tau) \end{cases}. \tag{3.32}$$

Even though this transport velocity is an order-ε^2 quantity, the fact that $k/L^2 \ll 1$ cancels out this effect, and we expect the flow to be significantly faster than the velocities in the gel, provided that $\varepsilon \gg \sqrt{k}/L$, equivalent to requiring $a_1 \gg \sqrt{k}$. Since k is of the order $10^{-15}\,\mathrm{m}^2$ or significantly smaller (Etzold *et al.* 2021), so this assumption is likely valid for all but nanoscale devices.

Figure 12 shows how the fluid pulse is centred on the thermal front, with the characteristic pulse width straightforward to deduce from the fitted front model of equation (3.27). Near

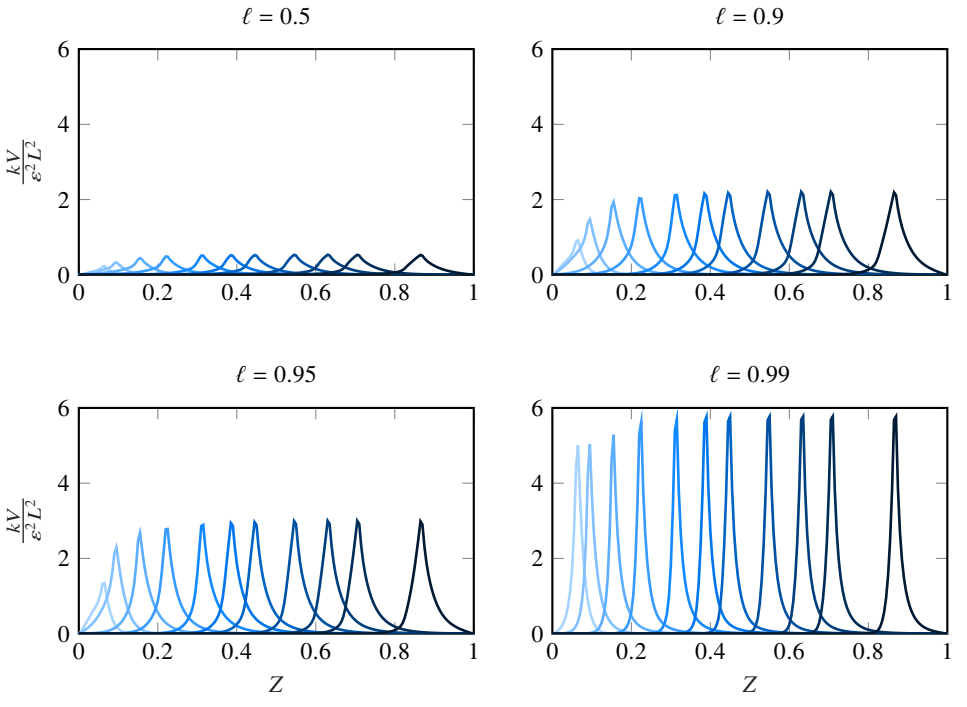

Figure 13: Plots of the scaled lumen velocities, repeating the approach of figure 12 for different values of ℓ, showing how the magnitude of the velocities is greater as ℓ is increased, but that the fluxes are more spatially localised in these cases. In all plots, time increases from the lighter to the darker curves.

$Z = Z_C$,

$$V \approx \frac{\varepsilon^2 L^2}{k} \frac{\ell^2 A(\ell) \Phi_1^{-2/3}}{16} (\Phi^* - 1) \operatorname{sech}^2 \left[A(\ell)(Z - Z_C)\right] \times \begin{cases} \tilde{\Pi} & Z < Z_C(\tau) \\ 1 & Z > Z_C(\tau) \end{cases}, \tag{3.33}$$

describing a translating pulse of characteristic width $A(\ell)^{-1}$ and maximum velocity magnitude

$$V_{\max} = \frac{\varepsilon^2 L^2 \ell^2 A(\ell)}{16k} \left(\frac{1 + \Phi^*}{2}\right)^{-2/3} \frac{1 + \tilde{\Pi}}{2}. \tag{3.34}$$

Thus, for sufficiently small $1 - \ell$, $V_{\max} \sim (1 - \ell)^{-1/2}$ and the pulse width $\sim (1 - \ell)^{1/2}$, and so the volume of fluid that can be transported by such a pumping action approaches a plateau as the tube gets thinner: even though transport is faster, the width of the pulse narrows. It is clear that increasing the lumen width both augments the transport capacity and response time to a heat pulse (up to a limit, since $\ell = 1$ corresponds to no tube). Figure 13 illustrates this exact behaviour, showing shorter, sharper, lumen flux pulses as the tube thickness is decreased. At values of ℓ very close to 1, the precise form of the flow field around the very thin tube walls must be considered, and the continuum approximations used in our present approach are likely invalid, so the precise manner in which fluid velocities approach zero cannot be elucidated. Our model is, however, valid for most thicknesses where such effects can be neglected.

4. Conclusion

Incorporating thermo-responsive effects into models of hydrogel swelling and drying can add a rich variety of new behaviours to already-complicated systems. In most thermo-responsive gels, raising the temperature above a critical threshold is seen to rapidly lower the affinity of the hydrophilic polymer chains for water molecules, and leads to a rapid increase in the equilibrium polymer fraction (the polymer fraction at which the osmotic pressure is zero). In this paper, we have extended the linear-elastic-nonlinear swelling model outlined in Webber & Worster (2023) to incorporate a temperature-dependent osmotic pressure that can reproduce this behaviour when the temperature is brought above the LCST threshold.

Starting from the thermodynamically-based models in common use in the literature (Hirotsu *et al.* 1987; Afroze *et al.* 2000; Cai & Suo 2011; Drozdov 2014), we show how a temperature-dependent Flory-Huggins interaction parameter χ leads to a temperature-dependent generalised osmotic pressure Π, and also elucidate the dependence of the shear modulus μ_s on the ambient temperature. These existing models are based on molecular-scale understandings of the interaction between water and polymer molecules, but the LENS theory that arises from this foundation is macroscopic in nature, and it is possible to choose much simpler, phenomenological, functional forms for $\Pi(\phi, T)$ and $\mu_s(\phi, T)$ that capture these behaviours without recourse to a complicated thermodynamic approach. Furthermore, applying this approach removes the need to understand the precise value of the interaction parameter, instead focusing on more easily measurable bulk-scale properties. We have also shown how key qualitative behaviours such as deswelling and changes in osmotic pressures can be captured by simpler, linearised, models of the same form used to model non-responsive gels (Doi 2009), allowing for qualitative predictions to be found analytically without any knowledge of the gel's micro-scale properties.

We then showed that the approach of the linear-elastic-nonlinear-swelling theory is able to reproduce the transient swelling or deswelling behaviour of thermo-responsive gels both qualitatively and quantitatively. By choosing functional forms for the osmotic pressure and shear modulus that fit the parameters used in Butler & Montenegro-Johnson (2022), we are able to use LENS to reproduce predictions from a full nonlinear Flory-Huggins approach, provided that no spinodal decomposition occurs. Our model also provides criteria for such phase separation to occur when the diffusivity – a function of macroscopic osmotic pressure and shear modulus – is negative, and dried and swollen gels can coexist adjacent to one another. In order to regularise solutions of the polymer fraction evolution equation in these cases, it is likely necessary to incorporate some kind of surface energy to penalise the formation of new surfaces (Hennessy *et al.* 2020), leading to Korteweg stresses at internal interfaces. The question of how to describe such an approach in the context of a LENS model remains a topic for future research, since the formation of sharp polymer fraction gradients is not permitted in LENS.

Some of the key applications of thermo-responsive hydrogels are hampered by the slow response times of such gels to changes in the ambient temperature. In general, hydrogel swelling or drying is a slow process, mediated by viscously-dominated interstitial flows through a low-permeability scaffold, with some gels taking hours or days to reach an equilibrium state (Bertrand *et al.* 2016). This is clearly undesirable in microfluidic devices or actuators, and having a tunable response time to changes in temperature may be desirable for certain applications (Maslen *et al.* 2023). In order to investigate the response time of simple gel structures, we have considered the case of a hollow tube of gel that can act like a displacement pump.

In this geometry, even though the axial dimension may be large, deformation timescales are set by the diffusion of water through the thin walls, so morphological changes can occur

much more rapidly than they would in a solid gel. This occurs because the shrinkage of the outside of the tube is no longer rate-limited by the need to deform and drive fluid through the interior of the gel, since water can flow relatively unimpeded down the lumen of the tube. The transport of water through the pipe-like structure that results can be used as a proxy measure of the speed of response, with water being transported large distances surprisingly quickly as a thermal signal propagates.

In order to model these tubes, we made a slenderness approximation that the polymer fraction varies axially at leading order, with only small radial corrections as water is expelled from the gel as the critical temperature threshold is exceeded. This allowed for a mathematical treatment similar to that used for transpiration through cylinders in Webber *et al.* (2023), and thus we can write down analytical expressions for all of the interstitial fluid fluxes in the gel and in the lumen. This approach allows us to tune the geometry of the tubes to match the exact response times desired, and allows for the computation of fluid flows through the pore matrix, along the axis of the tube, and out of the side walls.

Though there is no one way to measure the 'response time' in more complex geometries, we have discussed how varying the geometry and material properties of the gel that forms the tube lining can affect the speed at which fluid is transported through the lumen and the sharpness of the fluid pulse at the deswelling front. As one might expect, it is seen that thinner tubes react more rapidly to changes in temperature, and also that the resultant fluid pulse is more spatially localised around the thermal pulse in such cases. We have also elucidated the dependence of the fluid pulse driven down the pump on both the osmotic and elastic properties of the material forming the tube, allowing for the design of displacement pumps with specific response characteristics.

In the future, these simple model tubes could be connected together to form a network, propagating information about external stimuli through the medium of fluid pulses much more rapidly than in a solid block of hydrogel, forming the basis for a porous sponge built from porous hydrogel, with the pore size and geometry designed to match the desired material properties. Such an approach has already been taken experimentally in the design of microfluidic devices that exhibit dynamic anisotropy (Maslen *et al.* 2023), and we hope that our modelling will provide potential qualitative insights into the design characteristics of such devices in the future.

Acknowledgements. JJW thanks Matthew Hennessy and Matthew Butler for helpful discussions that led to the thermoelastic approach of appendix A, and Grae Worster for comments on a draft of the manuscript.

Funding. This work was supported by the Leverhulme Trust Research Leadership Award 'Shape-Transforming Active Microfluidics' (RL-2019-014) to TDMJ.

Declaration of interests. The authors report no conflict of interest.

Author ORCIDs. J. J. Webber, https://orcid.org/0000-0002-0739-9574; T. D. Montenegro-Johnson, https://orcid.org/0000-0002-9370-7720

Appendix A. Thermoelastic derivation of equation (2.11)

All hyperelastic models based on an energy density function $\mathcal{W}$ (the Helmholtz free energy) require an approach based on thermodynamics to derive the components of the stress tensor in terms of the deformation (Zaoui & Stolz 2001). Following a standard approach pioneered by Coleman & Noll (1963), we couple a law of local entropy imbalance with the expression for the rate of change of internal energy U,

$$T\frac{\mathrm{d}\eta}{\mathrm{d}t} \geqslant R - \boldsymbol{\nabla}\cdot\boldsymbol{Q} + \frac{1}{T}\boldsymbol{Q}\cdot\boldsymbol{\nabla}T \quad \text{and} \quad \frac{\mathrm{d}U}{\mathrm{d}t} = R - \boldsymbol{\nabla}\cdot\boldsymbol{Q} + \boldsymbol{P}\colon\frac{\mathrm{d}\boldsymbol{F}}{\mathrm{d}t} + \mu\frac{\mathrm{d}C}{\mathrm{d}t} - \boldsymbol{J}\cdot\boldsymbol{\nabla}\mu, \quad \text{(A 1)}$$

where η is the entropy, R is the external supply of heat, $\boldsymbol{Q}$ is the heat flux and T is the temperature, with all quantities measured per unit volume. $\boldsymbol{P}$ is the first Piola-Kirchhoff stress tensor given by

$$\boldsymbol{P} = \phi^{-1}\sigma\boldsymbol{F}^{-\mathrm{T}}, \tag{A 2}$$

with this term representing energy generation by elastic deformation. C is the number density of water molecules per unit volume of dry gel, equal to $(\phi^{-1}-1)/\Omega_f$, and μ is the chemical potential of the water. Finally, $\boldsymbol{J}$ is the molecular flux of water.

Since $U = \mathcal{W} + T\eta$, these two results can be combined into an inequality equivalent to the second law of thermodynamics, in the form of the Clausius-Duhem inequality. This indicates that the dissipation D must be greater than or equal to zero, where

$$D = -\frac{\mathrm{d}\mathcal{W}}{\mathrm{d}t} - \eta\frac{\mathrm{d}T}{\mathrm{d}t} + \mu\frac{\mathrm{d}C}{\mathrm{d}t} - \frac{1}{T}\boldsymbol{Q}\cdot\boldsymbol{\nabla}T - \boldsymbol{J}\cdot\boldsymbol{\nabla}\mu + \boldsymbol{P}\colon\frac{\mathrm{d}\boldsymbol{F}}{\mathrm{d}t}, \tag{A 3}$$

Using the chain rule and the form of $\mathcal{W}$ in equation (2.9) (i.e. an energy density that does not depend explicitly on $\boldsymbol{\nabla}T$),

$$\frac{\mathrm{d}\mathcal{W}}{\mathrm{d}t} = \frac{\partial\mathcal{W}}{\partial\mathsf{F}_{ij}}\frac{\mathrm{d}\mathsf{F}_{ij}}{\mathrm{d}t} + \frac{\partial\mathcal{W}}{\partial T}\frac{\mathrm{d}T}{\mathrm{d}t} + \frac{\partial\mathcal{W}}{\partial\phi}\frac{\mathrm{d}\phi}{\mathrm{d}t}, \tag{A 4}$$

Then, since $\mathrm{d}C/\mathrm{d}t = -(\mathrm{d}\phi/\mathrm{d}t)/(\Omega_f\phi^2)$,

$$\left(\frac{\partial\mathcal{W}}{\partial\mathsf{F}_{ij}} - \mathsf{P}_{ij}\right)\frac{\mathrm{d}\mathsf{F}_{ij}}{\mathrm{d}t} + \left(\frac{\partial\mathcal{W}}{\partial T} + \eta\right)\frac{\mathrm{d}T}{\mathrm{d}t} + \left(\frac{\partial\mathcal{W}}{\partial\phi} + \frac{\mu}{\Omega_f\phi^2}\right)\frac{\mathrm{d}\phi}{\mathrm{d}t} \leqslant \frac{1}{T}\boldsymbol{Q}\cdot\boldsymbol{\nabla}T + \boldsymbol{J}\cdot\boldsymbol{\nabla}\mu \tag{A 5}$$

Through the assumption that heat transfer and molecular transport are both Fickian, and follow laws of the form $\boldsymbol{Q} = \boldsymbol{A}\boldsymbol{\nabla}T$ and $\boldsymbol{J} = \boldsymbol{B}\boldsymbol{\nabla}\mu$ where both $\boldsymbol{A}$ and $\boldsymbol{B}$ are negative semidefinite matrices, the right-hand side is negative semidefinite, so the left-hand side must be less than or equal to zero. This inequality must hold for all deformations and values of $\partial T/\partial t$, so each bracketed term must be identically zero (Salençon 2007). Hence,

$$\eta = -\frac{\partial\mathcal{W}}{\partial T} \quad\text{and}\quad \boldsymbol{P} = \frac{\partial\mathcal{W}}{\partial\boldsymbol{F}} \quad\text{so}\quad \sigma = \phi\frac{\partial\mathcal{W}}{\partial\boldsymbol{F}}\boldsymbol{F}^{\mathrm{T}}. \tag{A 6}$$

Furthermore, the chemical potential μ is given by

$$\mu = \Omega_f\phi^2\frac{\partial\mathcal{W}}{\partial\phi}, \tag{A 7}$$

which, for the choice of $\mathcal{W}$ in equation (2.9), gives

$$\boldsymbol{\nabla}\mu = -\Omega_f\frac{\partial\Pi}{\partial\phi}\boldsymbol{\nabla}\phi, \tag{A 8}$$

with $\Pi(\phi)$ as in equation (2.15*a*). Since $\boldsymbol{\nabla}p = \Omega_f\boldsymbol{\nabla}\mu$ (Webber 2024), this shows that the thermodynamic model largely agrees with the transport equation (2.7) but neglects the contributions of shear to the polymer diffusivity.

Appendix B. Rewriting the poroelastic nonlinear model in the LENS formulation

In dimensional variables, the model of Butler & Montenegro-Johnson (2022) for the swelling of a gel sphere is

$$\frac{\partial \phi}{\partial t} = -\frac{k}{\mu_l \Omega_f}\frac{1}{r^2}\frac{\partial}{\partial r}\left(r^2\phi\frac{\partial \mu}{\partial r}\right) \quad \text{with} \tag{B 1a}$$

$$\frac{\partial \mu}{\partial r} = \Omega_f\left(\frac{\partial \sigma_r'}{\partial r} + \frac{\sigma_r' - \sigma_\theta'}{r} - \frac{\partial \Pi_{BMJ}}{\partial r}\right), \tag{B 1b}$$

where μ is the chemical potential, σ_r' and σ_θ' are the principal radial and polar stresses and Π_{BMJ} is the osmotic pressure as defined without contributions from isotropic elastic stresses, which can be related to the $\Pi(\phi)$ defined in equation (2.15*a*) via

$$\Pi_{BMJ} = \Pi(\phi) - \frac{k_B T}{\Omega_p}\left(\phi - \phi^{1/3}\right). \tag{B 2}$$

The nonlinear elastic principal stresses can be viewed as the effective stresses $\sigma_{rr} + p$ and $\sigma_{\theta\theta} + p$, and have the forms

$$\sigma_r' = \frac{k_B T}{\Omega_p}\left[\frac{(1-\xi_d/r)^2}{\phi} - \phi\right] \quad \text{and} \quad \sigma_\theta' = \frac{k_B T}{\Omega_p}\frac{\phi\xi_d}{r}\frac{2-\xi_d/r}{(1-\xi_d/r)^2}, \tag{B 3}$$

where ξ_d is the radial displacement from a fully-dry equilibrium. It is seen that

$$\frac{1}{\Omega_f}\frac{\partial \mu}{\partial r} = -\left(\frac{\partial \Pi}{\partial \phi} + \frac{k_B T}{3\Omega_p}\phi^{-2/3}\right)\frac{\partial \phi}{\partial r} + \frac{k_B T}{\Omega_p}\frac{\partial \phi}{\partial r} + \frac{\partial \sigma_r'}{\partial r} + \frac{\sigma_r' - \sigma_\theta'}{r}, \tag{B 4}$$

hence

$$\frac{\partial \phi}{\partial t} = \frac{k}{\mu_l}\frac{1}{r^2}\frac{\partial}{\partial r}\left\{r^2\left[\phi\frac{\partial \Pi}{\partial \phi} + \frac{4k_B T\phi_{00}^{1/3}}{3\Omega_p}\left(\frac{\phi}{\phi_{00}}\right)^{1/3}\right]\frac{\partial \phi}{\partial r}\right\} -$$

$$\frac{k}{\mu_l}\frac{1}{r^2}\frac{\partial}{\partial r}\left\{r^2\left[\frac{k_B T}{\Omega_p}\left(1+\phi^{1/3}\right)\frac{\partial \phi}{\partial r} + \frac{\partial \sigma_r'}{\partial r} + \frac{\sigma_r' - \sigma_\theta'}{r}\right]\right\}, \tag{B 5}$$

with the first two terms exactly equal to the LENS evolution equation (2.25) with diffusivity (2.28). The difference arises from the treatment of deviatoric strains, which are assumed to be small in the LENS model, with no such assumption made in this approach. If there are no deviatoric strains, and the gel is swollen to a uniform polymer fraction ϕ^*, it is clear that $\xi_d = (1-\phi^{*1/3})r$ and the second term is zero.

Otherwise, we can quantify the effect of the second term on the rate of change of ϕ in either swelling or drying contexts. Noting that

$$\frac{\partial \sigma_r'}{\partial r} + \frac{\sigma_r' - \sigma_\theta'}{r} = \hat{\boldsymbol{r}}\cdot\boldsymbol{\nabla}\cdot\sigma^{(\boldsymbol{e})} = \frac{1}{2\mu_s}\frac{\partial P}{\partial r} \tag{B 6}$$

When drying, $\partial\phi/\partial r > 0$ and we expect $\partial P/\partial r > 0$ as well, with the opposite effect when swelling. Thus, we expect real-world swelling to be faster than that predicted by the LENS model, with real-world shrinkage to be slower, once the full effects of deviatoric strains are incorporated.

The boundary condition at the gel–water interface in Butler & Montenegro-Johnson (2022)

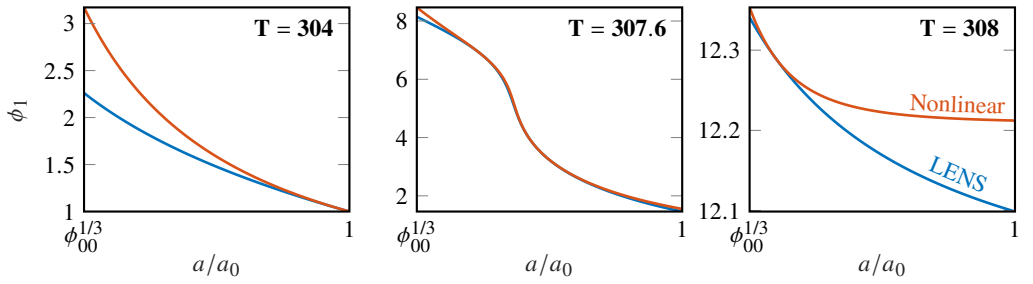

Figure 14: Comparison between the interfacial polymer fraction ϕ_1 at different temperatures as a function of bead radius a; in general, the bead has a drier interfacial state in the fully nonlinear model.

sets the local polymer fraction ϕ_1 via

$$\frac{a_0^4\phi_{00}^{\frac{4}{3}}}{a^4} - \phi_1^2 = -\Omega\phi_1\left[\phi_1 + \log(1-\phi_1) + \phi_1^2\chi - \phi_1^2(1-\phi_1)\frac{\partial\chi}{\partial\phi}\right] = \frac{\Omega_p\phi_1\Pi}{k_BT} - \left(\phi_1^2 - \phi_1^{\frac{4}{3}}\right). \tag{B 7}$$

This can be written

$$\begin{aligned}\Pi(\phi_1) &= \frac{k_BT}{\Omega_p}\left(\frac{a_0^4}{a^4}\frac{\phi_{00}^{4/3}}{\phi_1} - \phi_1^{1/3}\right)\\ &= 4\mu_s\left[\frac{a_0}{a} - \left(\frac{\phi_1}{\phi_{00}}\right)^{1/3}\right] + \mu_s\left[3\left(\frac{\phi_1}{\phi_{00}}\right)^{1/3} + \frac{a_0^4}{a^4}\frac{\phi_{00}}{\phi} - \frac{4a_0}{a}\right],\end{aligned} \tag{B 8}$$

which reduces exactly to the boundary condition of equation (2.29) in the case of no deviatoric strains (isotropic swelling with $a_0^3\phi_{00} = a^3\phi_1$). This modifies the interfacial polymer fraction from the value predicted by LENS theory, as illustrated in figure 14.

Appendix C. Comparison with linearised osmotic pressures

In later sections of this paper, we use the linearised form of the osmotic pressure in equation (2.24) to solve problems in an analytically-tractable form. In this appendix, we show that there is good qualitative agreement between the linearised model's predictions and those of the model employing the full osmotic pressure of (2.15*a*).

In the case of swelling with the temperature lowered from 308 K to 304 K, using the HHT parameters gives an osmotic pressure function that is zero at $\phi = \phi_{00}$, and close to zero for all small polymer fractions. This function is difficult to approximate linearly in the form of equation (2.24), as illustrated in figure 15a, but we show here how the resultant parameters still give good qualitative agreement with fully nonlinear calculations.

Using the lsqnonlin function in MATLAB to fit a value of Π_{00} (resulting in the linear osmotic pressure illustrated in figure 15a), we find that

$$\Pi_{00} = \frac{0.0824k_BT}{\Omega_f} \quad \text{and} \quad \mathcal{M} = 6.306\times10^{-3} \tag{C 1}$$

which can be substituted into a linearised form of the transport equation (2.25) with

$$D(\phi) = \frac{k\Pi_{00}}{\mu_l}\left[\frac{\phi}{\phi_0} + \frac{4\mathcal{M}}{3}\left(\frac{\phi}{\phi_0}\right)^{1/3}\right]. \tag{C 2}$$

(a) Comparison between nonlinear and linear expressions for $\Pi(\phi)$, where $\phi_0 = \phi_0(308\,\mathrm{K})$

(b) Plots showing the growth of the bead's radius

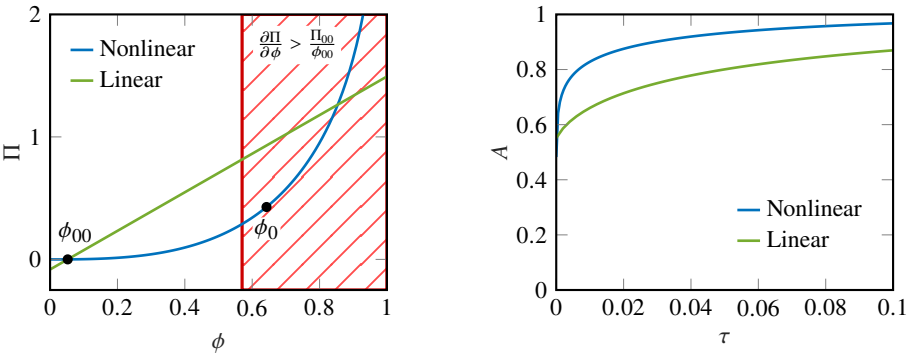

Figure 15: Plots comparing the fully nonlinear osmotic pressure model of Butler & Montenegro-Johnson (2022) with parameters from Hirotsu *et al.* (1987) with a fitted linear model of the form (2.24).

Figure 15b illustrates how swelling is slower in the case of linearised osmotic pressure than in the fully-nonlinear case computed by Butler & Montenegro-Johnson (2022). The reason for this difference in swelling rates is apparent in figure 15a: in drier gels (i.e. at the start of the swelling process), $\partial\Pi/\partial\phi$ is greater for the nonlinear osmotic pressure expression (the hatched region in the plot), so diffusion is more rapid here. This leads to faster growth relative to the fully-linear approach.

However, figure 15b shows that the same qualitative swelling behaviour is seen in the linearised case, justifying its use here for mathematical simplicity. All of the analysis in the present paper could be repeated with a nonlinear osmotic pressure if accuracy were required in timescales. Indeed, there is significant debate as to the accuracy of even the most commonly-accepted models for osmotic pressure at extremes of polymer fraction, where the gel may behave like more of a dilute suspension ($\phi \to 0$) or glassy material ($\phi \to 1$) (Feng *et al.* 2024). Other such functional forms for $\Pi(\phi)$, which often have a power-law dependence on polymer volume fraction, may be fitted more closely by a linear approximation around ϕ_{00}.

REFERENCES

Abramowitz, M. & Stegun, I. A. 1970 *Handbook of Mathematical Functions: with Formulas, Graphs, and Mathematical Tables*. National Bureau of Standards.

Afroze, F., Nies, E. & Berghmans, H. 2000 Phase transitions in the system poly(N-isopropylacrylamide)/water and swelling behaviour of the corresponding networks. *J. Mol. Struct.* **554** (1), 55–68.

Bertrand, T., Peixinho, J., Mukhopadhyay, S. & MacMinn, C. W. 2016 Dynamics of swelling and drying in a spherical gel. *Phys. Rev. Appl.* **6** (6), 064010.

Butler, M. D. & Montenegro-Johnson, T. D. 2022 The swelling and shrinking of spherical thermo-responsive hydrogels. *J. Fluid Mech.* **947**, A11.

Cai, S. & Suo, Z. 2011 Mechanics and chemical thermodynamics of phase transition in temperature-sensitive hydrogels. *J. Mech. Phys. Solids* **59** (11), 2259–2278.

Cai, S. & Suo, Z. 2012 Equations of state for ideal elastomeric gels. *EPL* **97** (3), 34009.

Coleman, B. D. & Noll, W. 1963 The thermodynamics of elastic materials with heat conduction and viscosity. *Arch. Ration. Mech. Anal.* **13** (1), 167–178.

Doi, M. 2009 Gel dynamics. *J. Phys. Soc. Jpn.* **78** (5), 052001.

Dong, L. & Jiang, H. 2007 Autonomous microfluidics with stimuli-responsive hydrogels. *Soft Matter* **3**, 1223–1230.

Drozdov, A. D. 2014 Swelling of thermo-responsive hydrogels. *EPJE* **37** (10), 93.

Etzold, M. A., Linden, P. F. & Worster, M. G. 2021 Transpiration through hydrogels. *J. Fluid Mech.* **925**, A8.

Feng, Y., Gerber, D., Heyden, S., Kröger, M., Dufresne, E. R., Isa, L. & Style, R. 2024 Characterizing hydrogel behavior under compression with gel-freezing osmometry. *arXiv preprint 2407.13718* .

Gomez, M., Moulton, D. & Vella, D. 2017 Critical slowing down in purely elastic 'snap-through' instabilities. *Nature Phys.* **13**, 142–145.

Guilherme, M. R., Aouada, F. A., Fajardo, A. R., Martins, A. F., Paulino, A. T., Davi, M. F. T., Rubira, A. F. & Muniz, E. C. 2015 Superabsorbent hydrogels based on polysaccharides for application in agriculture as soil conditioner and nutrient carrier: A review. *Eur. Polym. J.* **72**, 365–385.

Harmon, M. E., Tang, M. & Frank, C. W. 2003 A microfluidic actuator based on thermoresponsive hydrogels. *Polymer* **44** (16), 4547–4556.

Hennessy, M. G., Münch, A. & Wagner, B. 2020 Phase separation in swelling and deswelling hydrogels with a free boundary. *Phys. Rev. E* **101** (3), 032501.

Hirotsu, S., Hirokawa, Y. & Tanaka, T. 1987 Volume-phase transitions of ionized N-isopropylacrylamide gels. *J. Chem. Phys.* **87** (2), 1392–1395.

Lee, Y., Song, W. J. & Sun, J. Y. 2020 Hydrogel soft robotics. *Mater. Today Phys.* **15**, 100258.

Li, J., Hu, Y., Vlassak, J. J. & Suo, Z. 2012 Experimental determination of equations of state for ideal elastomeric gels. *Soft Matt.* **8** (31), 8121–8128.

Maslen, C., Gholamipour-Shirazi, A., Butler, M. D., Kropacek, J., Rehor, I. & Montenegro-Johnson, T. D. 2023 A new class of single-material, non-reciprocal microactuators. *Macromol. Rapid Commun.* **44** (6), 2200842.

Neumann, M., di Marco, G., Iudin, D., Viola, M., van Nostrum, C. F., van Ravensteijn, B. G. P. & Vermonden, T. 2023 Stimuli-responsive hydrogels: the dynamic smart biomaterials of tomorrow. *Macromolecules* **56** (21), 8377–8392.

Nistane, J., Chen, L., Lee, Y., Lively, R. & Ramprasad, R. 2022 Estimation of the Flory-Huggins interaction parameter of polymer-solvent mixtures using machine learning. *MRS Commun.* **12**, 1096–1102.

Peppin, S. S. L., Elliott, J. A. W. & Worster, M. G. 2005 Pressure and relative motion in colloidal suspensions. *Phys. Fluids* **17** (5), 053301.

Petersen, K. B. & Pedersen, M. S. 2012 The Matrix Cookbook, November 2012. *Technical University of Denmark* **7** (15).

Reddy, J. N. 2013 *An Introduction to Continuum Mechanics, Second Edition*. Cambridge University Press.

Richter, A., Klatt, S., Paschew, G. & Klenke, C. 2009 Micropumps operated by swelling and shrinking of temperature-sensitive hydrogels. *Lab Chip* **9**, 613–618.

Salençon, J. 2007 *Mécanique des milieux continus - II, Thermoélasticité*. Éditions de l'École Polytechnique.

Seo, J., Wang, C., Chang, S., Park, J. & Kim, W. 2019 A hydrogel-driven microfluidic suction pump with a high flow rate. *Lab Chip* **19**, 1790–1796.

Vernerey, F. & Shen, T. 2017 The mechanics of hydrogel crawlers in confined environment. *J. R. Soc. Interface* **14** (132), 20170242.

Voudouris, P., Florea, D., van der Schoot, P. & Wyss, H. M. 2013 Micromechanics of temperature sensitive microgels: dip in the Poisson ratio near the LCST. *Soft Matter* **9**, 7158–7166.

Webber, J. J. 2024 Dynamics of super-absorbent hydrogels. PhD thesis, University of Cambridge.

Webber, J. J., Etzold, M. A. & Worster, M. G. 2023 A linear-elastic-nonlinear-swelling theory for hydrogels. Part 2. Displacement formulation. *J. Fluid Mech.* **960**, A38.

Webber, J. J. & Worster, M. G. 2023 A linear-elastic-nonlinear-swelling theory for hydrogels. Part 1. Modelling of super-absorbent gels. *J. Fluid Mech.* **960**, A37.

Zaoui, A. & Stolz, C. 2001 Elasticity: Thermodynamic Treatment. *Encyclopedia of Materials: Science and Technology* pp. 2445–2448.

Zohuriaan-Mehr, M. J., Omidian, H., Doroudiani, S. & Kabiri, K. 2010 Advances in non-hygienic applications of superabsorbent hydrogel materials. *J. Mater. Sci.* **45** (21), 5711–5735.